Collision cross-sections and nonequilibrium viscosity coefficients of N_2 and O_2 based on molecular dynamics

Tapan K. Mankodi,[1, a)] Upendra V. Bhandarkar,[2] and R. S. Myong (명노신)[1]

[1)] *School of Mechanical and Aerospace Engineering and Research Center for Aircraft Core Technology, Gyeongsang National University, Jinju, South Korea*

[2)] *Department of Mechanical Engineering, Indian Institute of Technology Bombay, Mumbai, India*

(Dated: 20 February 2020)

This study examines collision dynamics of atom–atom, atom–molecule, and molecule–molecule interactions for O-O, N-N, O_2-O, N_2-N, O_2-N, N_2-O, O_2-O_2, N_2-N_2, and N_2-O_2 systems under thermal nonequilibrium conditions. Investigations are conducted from a molecular perspective using accurate O_4, N_4, and N_2O_2 ab-initio potential energy surfaces and performing Molecular Dynamics (MD) simulations. The scattering angle and collision cross-sections for these systems are determined, forming the basis for better collision simulations. For molecular interactions, the effect of the vibrational energy on the collision cross-section is shown to be significant, which in turn has a profound effect on nonequilibrium flows. In contrast, the effect of the rotational energy of the molecule is shown to have a negligible effect on the cross-section. These MD-based cross-sections provide a theoretically sound alternative to existing collision models, which only consider the relative translational energy. The collision cross-sections reported herein are used to calculate various transport properties, such as the viscosity coefficient, heat conductivity, and diffusion coefficients. The effect of internal energy on the collision cross-sections reflects the dependence of these transport properties on the nonequilibrium degree. The Chapman–Enskog formulation is modified to calculate the transport properties as a function of the trans-rotational and vibrational temperatures, resulting in a two-temperature nonequilibrium model. The reported work is important for studying highly nonequilibrium flows, particularly hypersonic re-entry flows, using either particle methods or techniques based on the conservation laws.

Keywords: Collision cross-sections, Molecular Dynamics–Quasiclassical trajectory, Nonequilibrium flows

[a)]Corresponding author: tapan.mankodi@iitg.ac.in; Also at Department of Mechanical Engineering, Indian Institute of Technology Guwahati, Guwahati, India

I. INTRODUCTION

There exists a need to understand the flow physics of re-entry vehicles traveling at hypersonic speeds in the rarefied regions of the atmosphere. The gas flow, predominantly consisting of molecular nitrogen and oxygen, undergoes rapid transformations around the strong bow shock formed in the forebody of such re-entry vehicles. These transformations may include inelastic collisions, chemical reactions (dissociation, Zeldowich exchange reactions, and recombination), ionization reactions, and excitation to higher electronic states. To study these processes, it is essential to have a better knowledge of the basic collision processes.

The Direct Simulation Monte Carlo (DSMC)[1,2] method is widely employed to simulate hypersonic flows around re-entry vehicles at rarefied ambient conditions. DSMC handles collisions using probabilistic models. There are several collision models that attempt to simulate the process in an accurate manner. One of the earliest, the Hard Sphere (HS) model, is straightforward in its implementation, but the resulting viscosity–temperature relation does not match experimental results. Bird[3] suggested the Variable Hard Sphere (VHS) model, an improved version of HS, in which the diameter is no longer a single-valued function, but instead depends on the relative speed of the collision. The values of the VHS parameters are chosen in such a way that the viscosity–temperature relation at a range about a reference temperature is accurate. This may lead to problems in applications involving a wider range of temperatures in the flow, as observed in problems involving shock structures. Other approaches such as the Variable Soft Sphere (VSS),[4] Generalized Hard Sphere (GHS),[5] and Generalized Soft Sphere (GSS)[6] models have attempted to improve the collision modeling. However, these models also have limitations due to their inherent phenomenological nature.

Several authors have reported alternative collision models that include the attractive component of the interatomic potentials. These models are more appropriate for investigating flows at low temperatures, where the attractive component has an important role to play. Matsumoto and Kuora[7] used the Lennard–Jones (LJ) potentials to study the velocity distribution functions in an argon shock wave, and Venkattraman et al.[8,9] presented an efficient algorithm for modeling the scattering angles using the LJ potential. Sharipov et al.[10,11] reported an ab-initio collision model that uses arbitrary intermolecular potentials such as the

LJ and Stockmayer potentials. A pre-calculated lookup table or deflection angle matrix was used to find the post-collision scattering angle instead of the analytical expression employed in the VSS model.

In summary, the following shortcomings can be attributed to existing collision models. First, the existing models are phenomenological and depend on several fitting parameters. Additionally, the collision cross-sections are assumed to be a function of only the translational energy of collision. It is evident that such models may handle atomic collisions accurately. However, extending this assumption to collisions involving molecules is questionable. The molecular diameter changes according to its rotational-vibrational (ro-vibrational) level, and this has a direct effect on the collision cross-sections. Recently, several authors have reported more fundamental chemical reaction models based on the reactive cross-sections[12–17] obtained using the Quasi-Classical Trajectory (QCT) method. The reported reactive cross-sections are known to depend on both internal energy and translational energy. However, few researchers[18,19] have acknowledged that it is questionable to apply ab-initio-based reaction models[20–26] when the collision models employed are a function of only the translational energy.

The present work attempts to address these shortcomings. The extent of the dependence of the collision cross-sections on the ro-vibrational levels of O_2-O, N_2-N, O_2-N, N_2-O and the O_2-O_2, N_2-N_2, N_2-O_2 interactions are examined. Unlike O-O or N-N interactions, the outcome of Molecular Dynamics (MD) simulations of scattering angles in atom–molecule or molecule–molecule interactions depends on many parameters. A different initial orientation of the molecule will result in a different value of the post-collision scattering angle for the same ro-vibrational level, impact parameter, and relative speed. Thus, an ensemble of different orientations is needed to gain a fair idea of the cross-section for any given combination of these values. This has to be followed by calculating the cross-sections for a large number of combinations of impact parameters, relative translational energies, and ro-vibrational levels. The collision cross-sections are tabulated in the supplementary material along with the scattering angle data.

In addition to the modeling of collisions, the collision cross-sections reported in the present work can be used in calculating transport coefficients through kinetic theory formulations. It is generally assumed that the transport properties are a function of translational temperature and nonequilibrium effects are generally neglected. In this study, the nonequilibrium effects

on the transport properties are investigated using the collision cross-sections. The accurate modeling of transport properties is important in simulating conservation laws, and this will have a wide range of applications in understanding nonequilibrium flows.

Section II discusses the MD procedures employed to calculate the scattering angles and collision cross-sections for atom–atom, atom–molecule, and molecule–molecule collisions. A detailed discussion of the scattering angles follows in Sect. III. The calculation of the collision cross-section in the case of atom–atom interaction is well established. In addition to the atom–atom collision cross-section results, the collision cross-section calculation method for atom–molecule and molecule–molecule collisions is described in Sect. IV. Along with these results, the viscosity–temperature relations under equilibrium conditions for the different colliding pairs are also provided. A discussion of the need for a nonequilibrium transport property model is presented in Sect. V. Finally, Sect. VI presents a summary of the key results.

II. MOLECULAR DYNAMICS CALCULATIONS

The time evolution of the position (q) and momentum (p) of atoms and molecules in MD simulations is traced by solving Hamilton's equation:

$$\dot{q} = \frac{\partial \mathcal{H}}{\partial p} = \frac{p}{m} \quad , \quad \dot{p} = -\frac{\partial \mathcal{H}}{\partial q} = -\frac{\partial \mathcal{V}}{\partial q} \tag{1}$$

In the present work, the $\mathcal{V}$ term, representing the potential energy surface (PES) of the system, is calculated using computational chemistry algorithms that solve Schrödinger's equation. MD simulations are carried out using O_4, N_4, and N_2O_2 PESs, many of which have been reported in recent years.[23,27–33] Among these, the one chosen for this study is the Complete Active Space Self Consistent Field (CASSCF)–Second-order Complete Active Space Perturbation Theory (CASPT2) triplet O_4 PES derived by Paukku et al.[32] for oxygen systems and the N_4 PES given by Paukku et al.[33] For the N_2-O_2 interaction, the CASSCF-CASPT2 N_2O_2 PES derived by Varga et al.[34] is employed. Six-dimensional permutationally invariant global least–square fits are available for these PESs.[35] The root mean square errors of the least–square fits for all points for the three N_4, O_4 and N_2O_2 PESs were found to be equal to 14.3, 5.6 and 7.8 kcal/mol respectively. Table I lists the computational details of the CASSCF-CASPT2 method and the structures for which the PESs are validated.

TABLE I. Details of CASSCF-CASPT2 PESs employed in the present work.

Collision Pair	System	Active electron/orbital	Points	PES used	Validation
N_2-N_2	N_4	12/12	16421	Paukku et al.[33]	Cyclic and Bent N_3 structure Tetrahedral N_4 structure
O_2-O_2	O_4	16/12	10180	Paukku et al.[32]	Cyclic O_3 structure O_3—O complex structure $(O_2)_2$ structure
N_2-O_2	N_2O_2	14/12	54889	Varga et al.[34]	C_{2v} and C_s NO_2 structure C_{2v}, $C_{\infty v}$ and $D_{\infty h}$ N_2O structure C_{2v} N_2O_2 structure

The QCT/MD code employed in the present work is an extension of our previous code implemented to calculate the reaction cross–sections for ab-initio based chemical reaction model. The in–house code was validated thoroughly[22]. The procedure of using MD to find scattering angles of atom–atom (N–N and O–O collision pair) collisions, which subsequently are used to obtain collision cross-sections is as follows. One of the two atoms is initially placed at the origin, while the second is projected towards the first with a known relative speed (c_r) and an impact parameter (b). The initial separation between the two atoms is 20 Å. Since the PESs used are for four atom systems, it is assumed that the remaining atoms of the system that are not participating in the interactions are placed far away such that they do not influence the colliding atom–atom pair in question. The standard second-order Verlet algorithm with an adaptive time-step is used as a time integrator. It is ensured that the time step is never greater than 1×10^{-16} s. In case of atom–atom collisions, the relative speed ranges from 200–20 000 m/s, and the impact parameter is iteratively increased by 0.1 Å until there are no more interactions between the two particles. The simulation is said to be complete when the distance between the two atoms after the collision exceeds the

initial interatomic distance. The simulations are repeated for a large number of relative speeds and impact parameters. The potential energy curve between the O–O and N–N pair asymptotes at a large distance and hence it is necessary to define a reasonable cut-off distance or threshold impact parameter beyond which, it can be presumed that there is no interaction between the two particles. It is assumed that simulations in which the scattering angle is less than 1° have not undergone any collision.

In the case of atom–molecule collisions, for a given combination of relative speed, ro-vibrational level of the molecule, and impact parameter, the scattering angle depends on the orientation of the molecule. Thus, the dynamical study of molecular collisions requires ensembles of MD simulations with randomly sampled initial orientations of the molecule, which will result in a distribution of scattering angles. In this aspect, the present molecular simulations are similar to the QCT method employed for calculating reactive cross-sections.[36,37] Initially, the molecule is positioned in such a manner that its center coincides with the origin of the coordinate system. The atoms constituting the molecules are placed on either direction of the origin such that the interatomic distance is equal to either one of the turning radii ($r_{\pm}$). The turning radii are calculated by solving the vibrational Schrodinger equation using the semi-classical Wentzel-Brillouin-Kramers (WKB) method. Unlike atom–atom interaction, the atom–molecule system is not restricted to planar geometry. The scattering angle has both polar and azimuthal components. However, in the present study, the initial orientation and momentum of the molecule are randomly chosen, and the distribution of the polar component of the scattering angle is expected to be isotropic. In the following text, the scattering angle is represented using only the azimuthal component.

Ensembles consisting of a large batch of trajectories are run for a vast number of ro-vibrational levels, relative speeds, and impact parameters. All vibrational levels ($v_{max}(N_2) = 56$ and $v_{max}(O_2) = 36$) from the zeroth to the highest levels are included. At each vibrational level, two rotational levels (zeroth and half the maximum permissible rotational level for the particular vibrational level) are included. Twenty-five relative speeds ranging from 100–20 000 m/s are considered.

In the case of molecule–molecule interactions, the ro-vibrational energy levels of both molecules need to be considered. The analysis of atom–molecule interactions show that the rotational levels do not seem to have a significant effect (as will be described in a later section). Hence, only different vibrational levels are considered for the molecule–

molecule interactions, and the rotational level is fixed at the ground state. The ensembles are generated for cases with: (1) v_1 = N and v_2 = 0 $\in$ {0, 1, 2, 3, ..., 36} and (2) v_1 = v_2 = N $\in$ {0, 1, 2, 3, ..., 36} for O_2-O_2 collisions. In the case of the N_2-N_2 system, the maximum vibrational level considered is 48. The number of grid points in the relative velocity and impact parameter dimensions is the same as that considered for the atom–molecule simulations.

The MD simulations are run in parallel on a 12-core Intel Xeon machine. Each atom–atom simulation takes approximately 16.23 s (O-O) and 15.6 s (N-N). It is evident that the atom–atom simulations are not resource- or time-consuming. Each atom–molecule simulation takes approximately 25 s (O_2-O) and 22.2 s (N_2-N). The increase in computational cost is understandable due to the additional atom in the system. Single molecule–molecule simulations for the O_2-O_2 and N_2-N_2 interactions take approximately 41 s and 40 s, respectively. In comparison, the computational cost for N_2-O_2 collisions is 62 s. This increase is caused by the higher number of terms in the fitting function of the N_2-O_2 PES. The drastic increase in the total computational time in the case of atom–molecule and molecule–molecule collisions in comparison to the atom–atom case is due to the sampling of trajectories and the higher number of input dimensions.

III. SCATTERING ANGLE RESULTS

The collision dynamics of atom–atom interactions are well established, and so we move on to discuss the scattering angle distribution in the case of atom–molecule systems. Figure 1 shows histograms of the distribution of scattering angle for the zeroth and 20th vibrational levels for O_2-O collisions. For the two vibrational levels, subfigures 1(a), 1(c), and 1(e) show the distribution at lower relative speed (V_R = 850 m/s) and subfigures 1(b), 1(d), and 1(f) show the distribution at higher relative speed (V_R = 2500 m/s). For each subfigure, histograms are shown at two different rotational levels (j=0, 121 for v=0 and j=0, 71 for v=20) for each of the two vibrational levels considered. Figures 1(a) and 1(b) depict the distribution of the scattering angle with an impact parameter of 0.1Å. At this lower impact parameter, the distribution of the scattering angle is skewed towards 180° because all the interactions between the incoming atom and the molecule are head-on collisions. With an increase in the impact parameter, the peak of the distribution shifts towards the center,

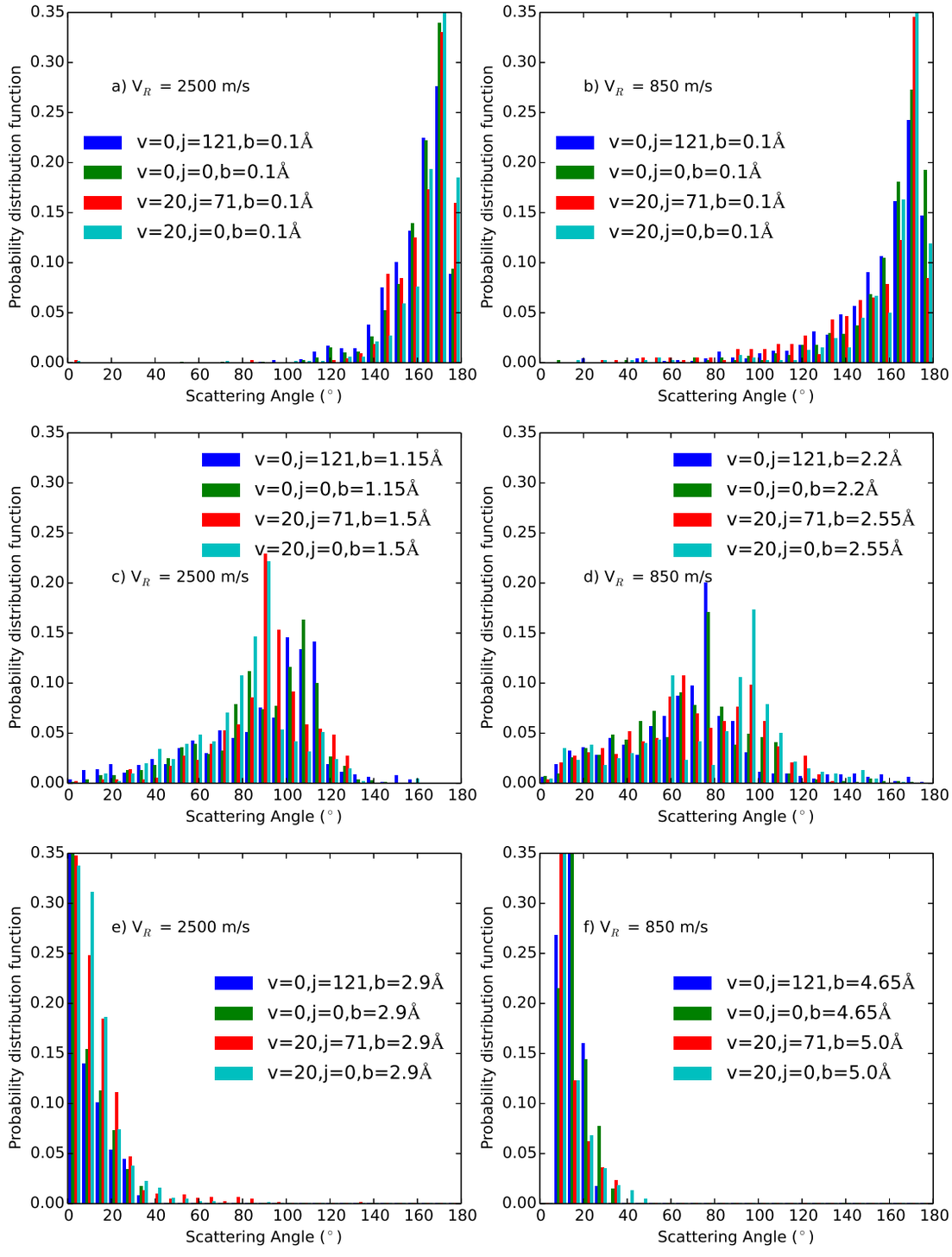

FIG. 1. Histograms of scattering angles for zeroth and 20$^{\text{th}}$ vibrational level, two rotational levels (zeroth and half the maximum rotational level at the given vibrational level), and different relative speeds and impact parameters for O_2-O collisions.

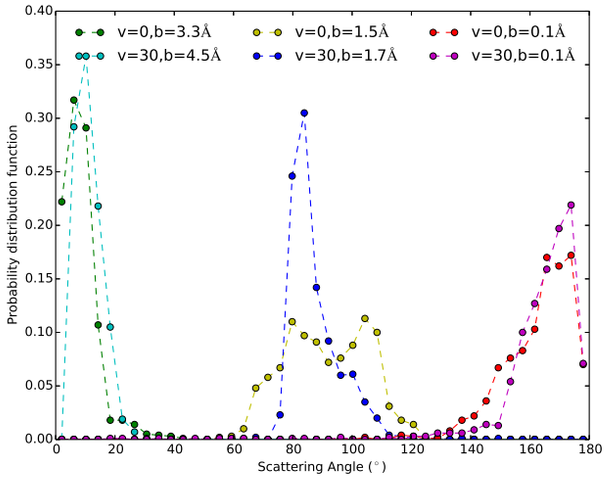

FIG. 2. Line plots of distribution of scattering angles for different vibrational levels and impact parameters (at relative velocity $V_R = 2500$ m/s) for O_2-O_2 collisions.

as can be seen in Figs. 1(c) and 1(d). Subfigures 1(c) and 1(d) depict histograms at impact parameters equal to 1.15 Å and 2.2 Å, respectively, for the zeroth vibrational level. With a further increase in the impact parameter, the distribution of scattering angle shifts towards 0°, and finally the distribution is skewed with a peak at 0°. Figures 1(e) and 1(f) show histograms of the distribution of scattering angle skewed towards 0°. The impact parameters for these subfigures are 2.55 Å and 3.25Å, respectively, for the zeroth vibrational level. The histogram in such cases is a single-valued function peaking at 0°. The value of the maximum impact parameter increases with a decrease in the relative speed. As the relative speed increases, the interaction time between the colliding particles decreases, leading to less chance of scattering. As shown in each subfigure of Fig. 1, the difference in the distribution of scattering angles at the two rotational levels is unclear and insignificant. The pattern of the histograms, initially skewed around 180° at lower values of the impact parameter and shifting towards 0° with an increase in impact parameter, is also observed at higher vibrational levels. Similar trends can also be observed for N_2-N, O_2-N, and N_2-O collisions.

Figure 2 shows the distribution of scattering angle for simulations at 2500 m/s relative speed for O_2-O_2 collisions. The results and analysis for the distribution of scattering angle in molecule–molecule simulations are similar to those observed for the atom–molecule simulations. At lower values of the impact parameter (=0.1 Å), the shape is skewed towards 180°. As the impact parameter increases, the distribution peak moves towards lower scattering

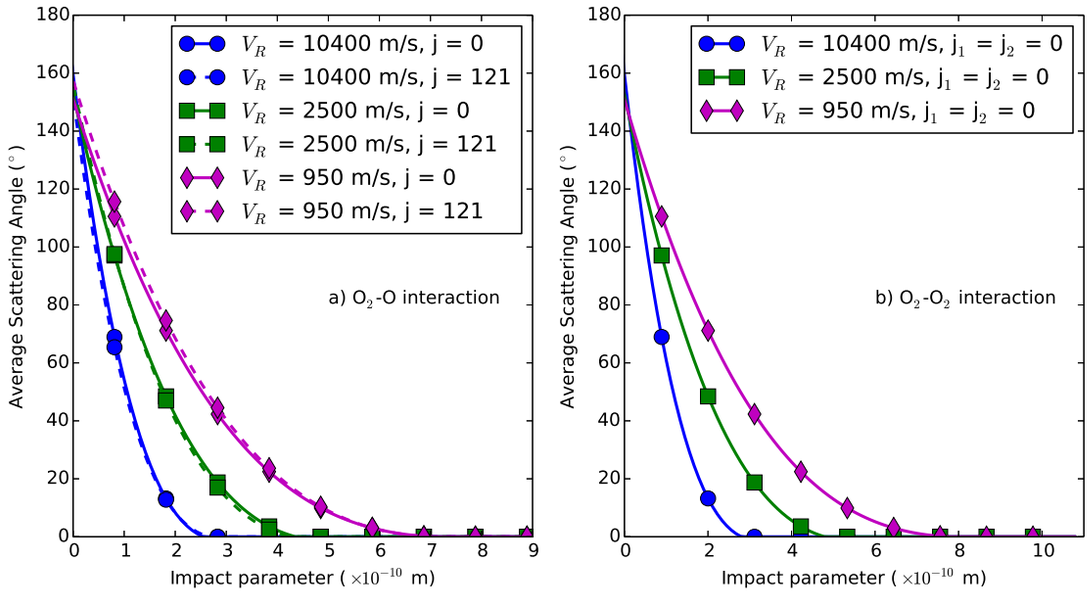

FIG. 3. Line plot of average scattering angles with respect to impact parameter for different relative speeds and ro-vibrational levels for (a) O_2-O and (b) O_2-O_2 interactions.

angles and becomes centered around 90°. Note that the centered distribution corresponds to different impact parameters for the two vibrational levels. Here, the impact parameter employed for the higher vibrational level is greater than that for the zeroth vibrational level. Any further increase in impact parameter skews the distribution farther toward 0°. Again, the value of the impact parameter is higher (=4.5Å) for the scattering angle distribution at the 30th vibrational level than at the zeroth vibrational level (=3.3Å). Similar trends can be observed for the other two systems.

Figure 3(a) shows the variation in average scattering angle for all simulations, comprising an ensemble with respect to the impact parameter for different relative speeds and ro-vibrational levels for O_2-O collisions. Figure 3(a) shows the variation at the zeroth vibrational level. Note that at higher relative speeds, the threshold value of the impact parameter at which the average scattering angle decreases to 0° is lower than that observed for ensembles with a lower relative speed. The difference between the average scattering angle plots for different rotational levels (but with the same relative speed and vibrational level) is insignificant. It is safe to presume that the rotational level of the molecule has an inconsequential effect on the scattering angle and, further, on the collision cross-section. Again, similar observations are noted for other atom–molecule collisions.

Line plots of the average scattering angle with respect to the impact parameter for O_2-O_2 collisions are shown in Fig. 3(b) for the zeroth vibrational level. As expected, the threshold impact parameter at which the average scattering angle is less than 1° increases as the relative speed decreases. Note that for the same relative speed, the value of the threshold impact parameter for the molecule–molecule interactions is greater than that for the atom–molecule interactions. This is primarily due to the difference in the PES when O_3 and O_4 systems are considered, wherein the molecular orbitals of O_2 disperse farther from the center than the atomic orbitals of O, which is to be expected. Thus, molecule–molecule interactions have a longer field of influence than atom–molecule interactions.

IV. CROSS-SECTION CALCULATIONS AND VISCOSITY–TEMPERATURE RELATIONS

A. Atom–Atom Interactions

The differential cross-section is defined[38]as:

$$\sigma = \frac{b}{sin\theta}\left|\frac{db}{d\theta}\right| \tag{2}$$

where b is the impact parameter and θ is the scattering angle. The collision cross-section is calculated by integrating the differential cross-section as follows:

$$\sigma_T = 2\pi \int_0^{\pi} \sigma sin\theta d\theta \tag{3}$$

The variations in the collision cross-sections as a function of relative speed for the O-O and N-N systems are shown in Figs. 4(a) and 4(b), respectively. In addition to the ab-initio collision cross-sections, Fig. 4 also shows a comparison with the two VHS cross-sections for O-O and N-N collisions established by Bird[39] and Svehla et al.[40] For both systems, at lower relative speeds, the MD-based collision cross-sections are greater than the VHS cross-sections. In contrast, at higher relative speeds, the values of the MD-based collision cross-section are lower than the VHS cross-sections reported by Svehla et al. For high-temperature calculations, it has been asserted[41] that the VHS parameters used by Svehla et al.[40] are more appropriate than those suggested by Bird.[39] This opinion is validated in the present work. However, at low speeds in the range of 100–250 m/s, the VHS parameter

provided by Svehla et al. underpredicts the collision cross-section and the VHS parameters provided by Bird are more reliable. The insets in Fig. 4 highlight this recommendation. The better match with Bird's results at lower temperatures seems to be a direct consequence of the choice of a lower reference temperature by Bird (298 K).

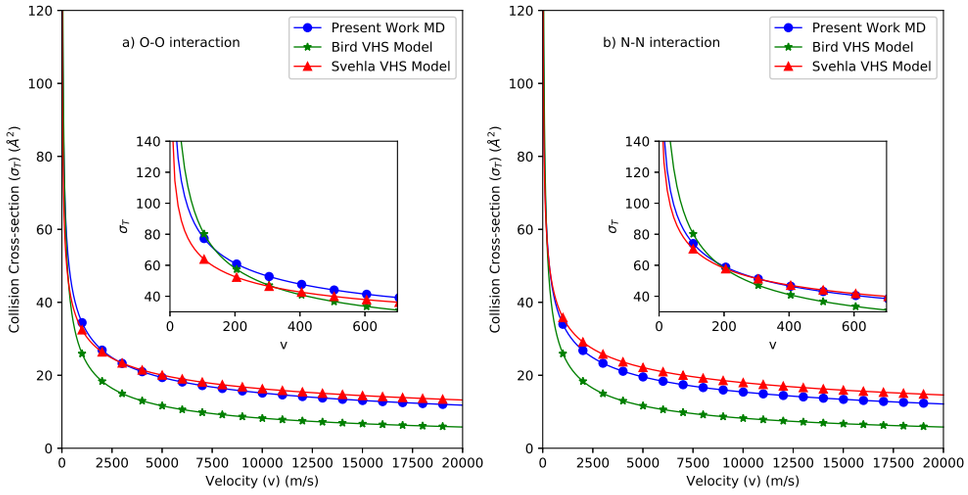

FIG. 4. Comparison of the variation of collision cross-section (σ_T) for (a) O-O system and (b) N-N system with relative speed calculated in the present work against previously established VHS cross-sections.

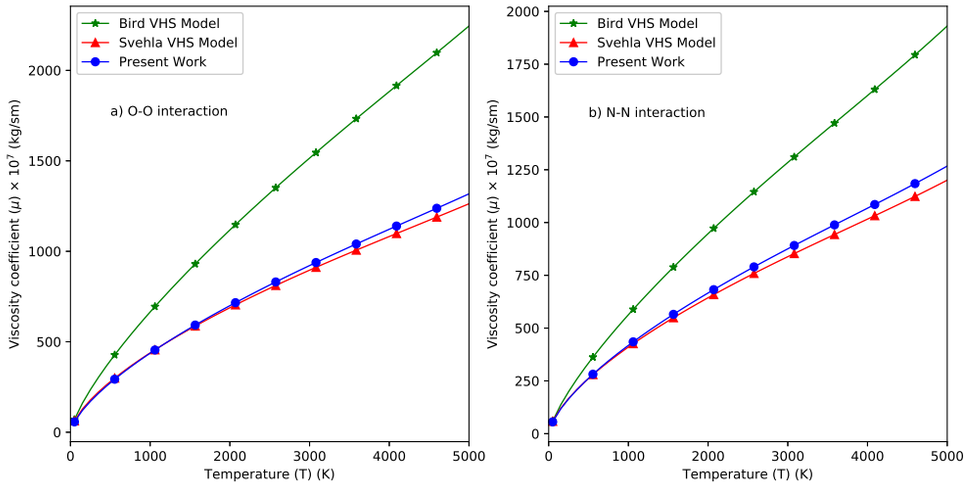

FIG. 5. Coefficient of viscosity as a function of temperature for (a) atomic oxygen and (b) atomic nitrogen. The present calculations are compared with previously established VHS relations.

The collision cross-section can be further used to calculate the first-order approximation

of viscosity–temperature dependence.[38]

$$\mu = \frac{(5/8)(\pi m k T)^{1/2}}{(m/(4kT))^4 \int_0^\infty c_r^7 \sigma_\mu exp[-mc_r^2/(4kT)]dc_r} \tag{4}$$

where m is the reduced mass, k is the Boltzmann constant, c_r is the relative speed and σ_μ is the viscosity cross-section which is given by the following relation:

$$\sigma_\mu = 2\pi \int_0^\pi \sigma sin^3\theta d\theta \tag{5}$$

Figures 5(a) and 5(b) show the variation in the coefficient of viscosity with respect to temperature for different cross-section data for atomic oxygen and atomic nitrogen, respectively (calculated using the present cross-section data and using existing VHS parameters). For both systems, the coefficients of viscosity calculated using the collision cross-section data in the present work are closer to those obtained using the VHS parameters provided by Svehla et al. than with those provided by Bird, again affirming the validity of Svehla's data, especially at high temperatures.[41] It must be clarified that the comparison of collision cross–sections and viscosity–temperature dependence at high temperatures calculated in the present work with those obtained using parameters recommended by Bird are to highlight a wide contrast between the two models since Bird's VHS parameters were calibrated to near ambient temperature conditions only.

In addition to the shear viscosity, the bulk viscosity plays an important part in the shock structures in polyatomic gas flows at high temperature adding to the complexity of the problem. The bulk viscosity coefficient is a measure of the dilatational stresses which is caused by the collisional relaxation of the internal modes: rotational and vibrational levels. The rotational modes of gas molecules are excited even at room temperature, making it ubiquitous across all flow conditions. The rotational non-equilibrium effect can be accounted for by introducing the excess normal stress associated with bulk viscosity[42–45]. In this framework, the effect of bulk viscosity can be treated by determining the ratio of the bulk viscosity to the shear viscosity. On the other hand, QCT modelling of rotational and vibrational relaxation, and calculation of inelastic collision cross–sections will provide better insight in theoretical calculation of bulk viscosity coefficient. The present work is limited to calculation of coefficient of shear viscosity, while the effect on bulk viscosity will be addressed in a future work.

B. Atom–Molecule and Molecule–Molecule Interactions

In the case of atom–atom interactions, there exists an established formulation for calculating the collision cross-section. However, in the case of atom–molecule and molecule–molecule interactions, the same formulation cannot be employed to calculate the collision cross-section. First, it is necessary to define a cut-off distance for the impact parameter that can be used to calculate the cross-sections. In the present model, the collision cross-sections are defined as follows:

$$\sigma_T(v, j, V_R) = \pi b_{max}^2 \tag{6}$$

where b_{max} is the threshold value of the impact parameter at which the average scattering angle of a simulation ensemble is less than 1°. In the case of atom–molecule interactions, the total number of σ_T required would be equal to the number of vibrational levels of the diatomic molecule. For the case of molecule–molecule interactions belonging to same species, the number of σ_T required is $N_{vib} \times (N_{vib} - 1)/2$, where N_{vib} is the number of vibrational levels of the molecules.

The collision cross-section as a function of relative translational velocity for a particular combination of a ro-vibrational level is best approximated using a fit of the following form:

$$\sigma_{T,fit}(v, V_R) = a(v) V_R^{b(v)} \tag{7}$$

where a and b are fitting parameters. These parameters are different for each vibrational level. The subscript j can be dropped from the fit as the rotational level of the molecule does not affect the scattering angle distribution and, subsequently, the collision cross-sections. In a semi-logarithmic scale along the V_R dimension, the behavior of the collision cross-section with respect to the relative speed produces a downward-sloping straight line. This form of collision cross-section relation can be adjusted in such a way that the viscosity calculated at two temperatures accurately matches existing valid data. The parameters of the collision cross-section fits are adjusted as:

$$\sigma_{T,adj}(v, V_R) = (a(v) + a') V_R^{b(v)+b'} \tag{8}$$

where it is assumed that a' and b' have a single value for the system and are independent of the vibrational level.

The viscosity calculations in the case of atom–molecule and molecule–molecule systems are approximated in the following form due to the inclusion of the vibrational level:

$$\mu = \frac{(5/8)(\pi m k T)^{1/2}}{(\frac{m}{4kT})^4 Q_v^{-1}[\sum_{v_1,v_2} exp(-\frac{E_{v_1}}{kT}) exp(-\frac{E_{v_2}}{kT}) \int_0^\infty c_r^7 \frac{2}{3} \sigma_{T,adj}(v_1, v_2) exp(-\frac{m c_r^2}{4kT}) dc_r]} \tag{9}$$

where E_{v_1} and E_{v_2} are the vibrational energies of the two molecules at v_1 and v_2 vibrational levels respectively, and Q_v is the partition function for the vibrational degree of freedom:

$$Q_v = \sum_{v_1,v_2} exp(-\frac{E_{v_1}}{kT}) exp(-\frac{E_{v_2}}{kT}) \tag{10}$$

In the case of atom–molecule collisions, a single summation over the vibrational levels of the molecule is computed. The temperature values employed to calculate the adjusted parameters for O_2-O_2, N_2-N_2, and N_2-O_2 systems are 273.15 K and 293.15 K. The corresponding viscosity data at these temperatures are obtained from the NIST data.[46] For atom–molecule collision systems, Wilke's mixing rule[47] is employed to obtain the mixture viscosities for the same set of temperatures. The values of the adjusted parameters in Equation 8 are calculated using back substitution in Equation 9 and the collision cross-sections are modified accordingly. The viscosity given by this method of fitting is in good agreement with those provided by the NIST database at temperatures up to 1000 K.

Figures 6(a)–6(d) show the variation of collision cross-section calculated in the present work for O_2-O, N_2-N, O_2-N, and N_2-O collisions, respectively, at different vibrational levels. The VHS cross-section data using the parameters proposed by Bird[39] and Svehla et al.[40] are also plotted. The collision cross-section data at the zeroth vibrational level for both the systems calculated in the present work are closer to the VHS cross-section data employing the parameters proposed by Svehla et al. than with those predicted by the parameters reported by Bird. Surprisingly, the differences between the cross-sections for O_2-O and O_2-N and for N_2-N and N_2-O are negligible.

Similarly, Figs. 7(a)–7(c) show the variation in total molecule–molecule cross-sections calculated in the present work under different combinations of vibrational levels for O_2-O_2, N_2-N_2, and N_2-O_2, respectively. Additionally, the figures show the VHS cross-sections using the parameters reported by Bird[39] and Svehla et al.[40]. For all three systems (O_2-O_2, N_2-N_2, and N_2-O_2), it is clear that the collision cross-sections calculated for different vibrational level combinations have significant differences. Similar to the atom–molecule systems, the cross-sections calculated using Svehla's VHS parameters are closer to the cross-sections obtained in the present work with both molecules occupying the zeroth vibrational

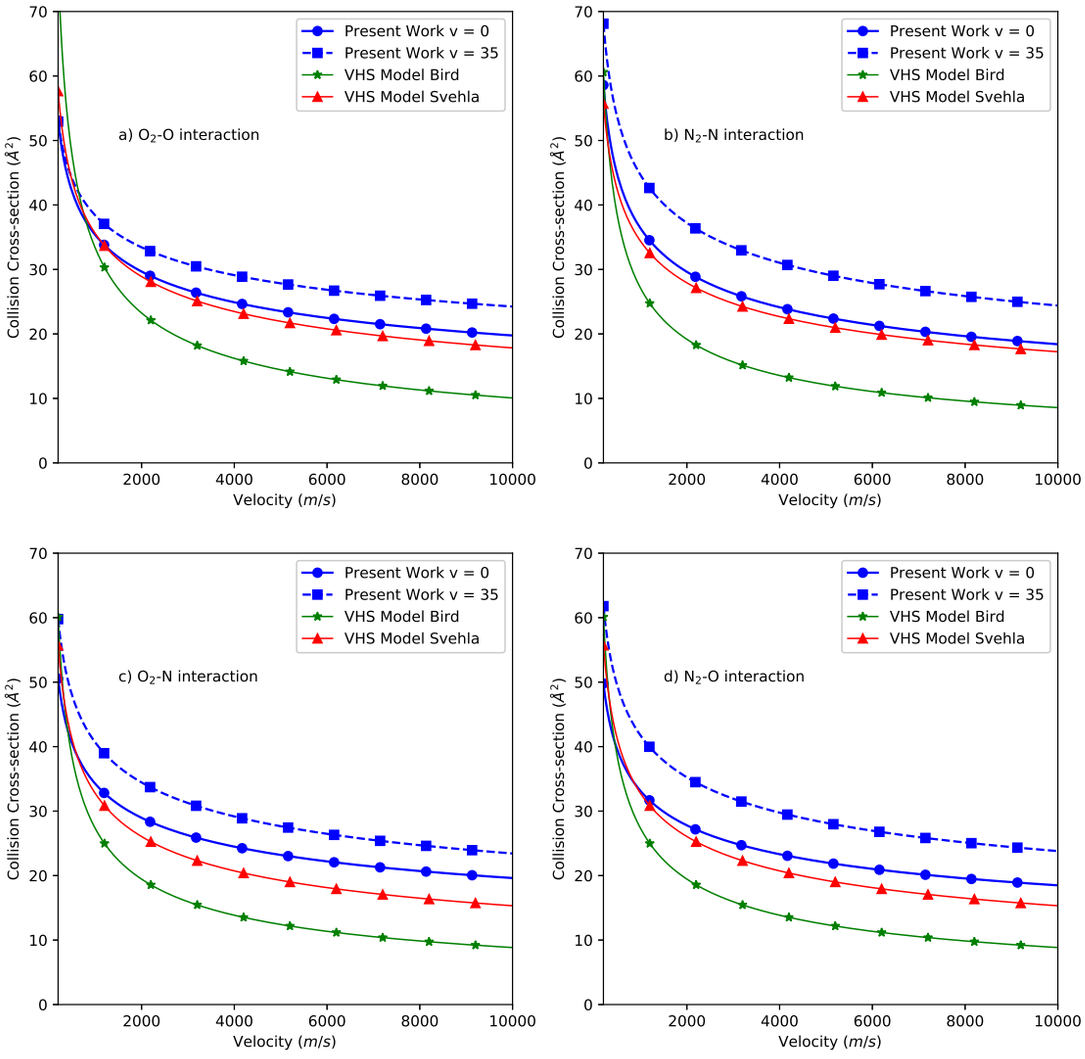

FIG. 6. Line plots of collision cross-section for (a) O_2-O, (b) N_2-N, (c) O_2-N, and (d) N_2-O interactions with respect to relative speed for different vibrational level combinations calculated in the present work.

level when compared with those calculated using Bird's VHS parameters. This also indicates that Svehla's parameters remain effective at higher temperatures. However, the differences in the collision cross-sections for different combinations of vibrational levels are explicit.

In the case of N_2-O_2 collisions [shown in Fig. 7(c)], the collision cross-sections for the $v_1 = v_{N_2} = 35$ and $v_2 = v_{O_2} = 0$ combination is greater than that for the $v_1 = v_{N_2} = 0$ and $v_2 = v_{O_2} = 35$ combination. A nitrogen molecule in the 35th vibrational energy level has more energy than an oxygen molecule in its 35th vibrational level. This shows

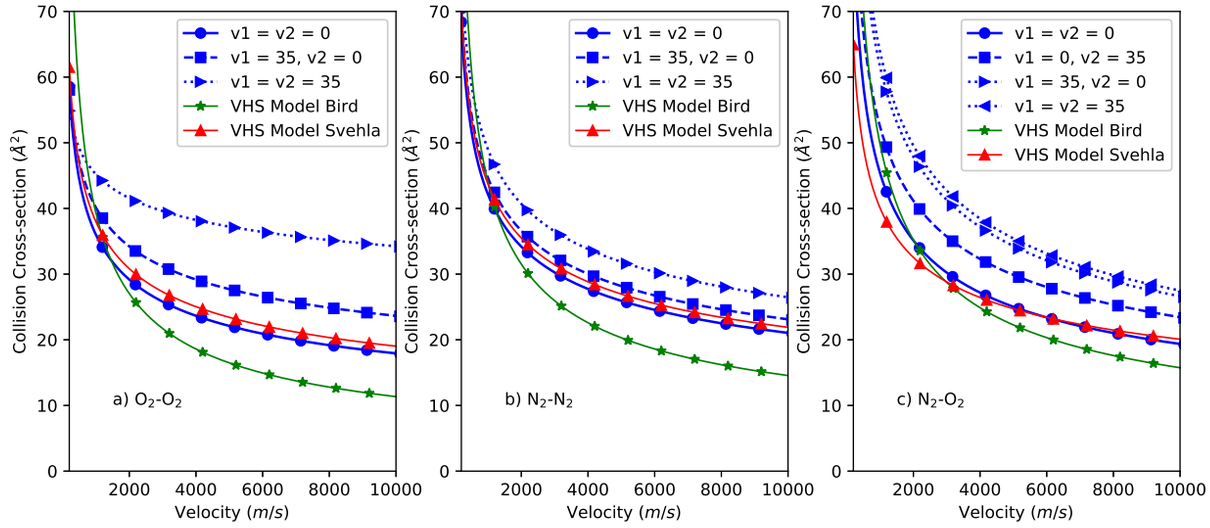

FIG. 7. Line plots of collision cross-section for (a) O_2-O_2, (b) N_2-N_2, and (c) N_2-O_2 interactions with respect to relative speed for different vibrational level combinations calculated in the present work.

that the vibrational energy has a significant effect on the collision cross-sections and that the combination of vibrational levels in a hetero-molecular interaction, such as for N_2-O_2 systems, is important.

Figures 8(a)–8(c) show the variation in the coefficient of viscosity with respect to temperature by integrating the collision cross-sections obtained in the present work and the VHS cross-sections for molecular oxygen, nitrogen, and a mixture of oxygen and nitrogen in equal proportion, respectively. Note that the viscosity–temperature relationship obtained in the present work matches perfectly with those obtained using VHS parameters at temperatures up to 800 K. Beyond 800 K, the viscosity coefficients predicted with the Svehla VHS model are lower than the predictions from the present work. The present viscosities also match quite well with those provided by Blottner et al.[48] and Boushehri.[46] For N_2-O_2 collisions, Wilke's mixing formula is employed to obtain the effective viscosity using Blottner's data for molecular nitrogen and oxygen.

The adjusted parameters introduced in Eq. (8) to modify the collision cross-sections were calculated on the basis of two temperature values and the corresponding viscosities. However, the viscosity–temperature relation calculated in the present work matches the NIST data well over the entire range of temperatures. The formulation of the adjusted parameters

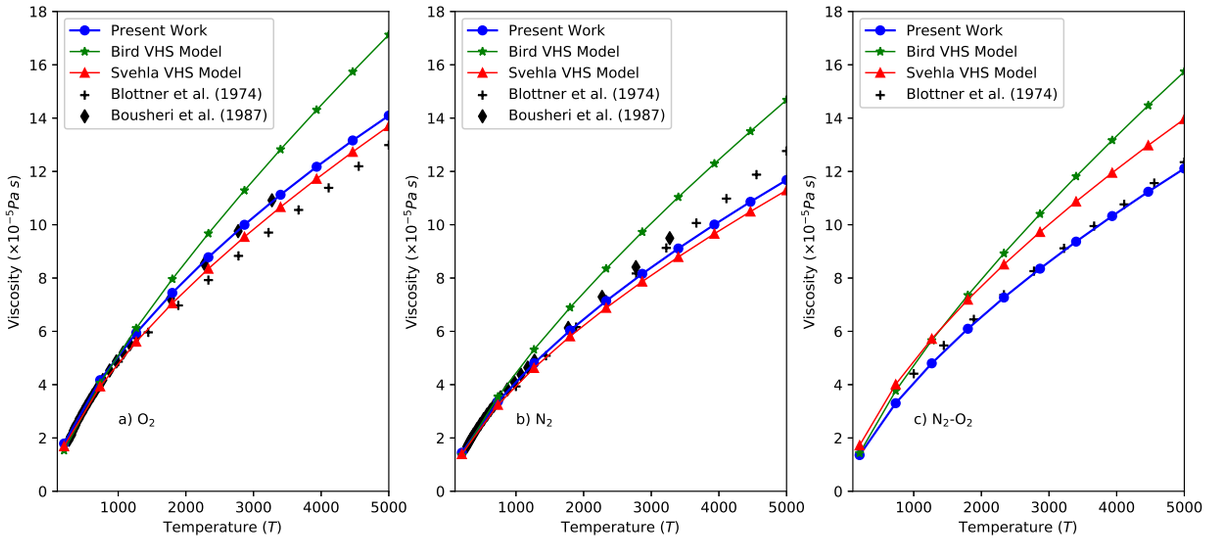

FIG. 8. Viscosity–temperature relations obtained from the present collision cross-sections for (a) molecular oxygen, (b) molecular nitrogen, and (c) mixture of nitrogen and oxygen at equal mole fractions compared with those calculated using previously established VHS cross-sections and viscosity models.[46,48]

employed in the collision cross-section calculations should therefore be assessed. In the absence of a convincing theory for calculating the collision cross-sections for atom–molecule and molecule–molecule interactions, as a first approximation, the proposed formulation is reasonable.

C. Effect of vibrational level dependent collision cross–sections on re-entry flows

The collision cross-sections calculated for higher vibrational levels in the present work are remarkably different from those predicted by the VHS cross-sections. It is also apparent that the vibrational level has a notable effect on the collision cross-section, especially at higher relative speeds. The collision cross-sections at higher vibrational levels are larger than those at lower vibrational levels. This will have a profound effect on hypersonic nonequilibrium flows, particularly re-entry flows. Towards this end, the vibrational level dependent collision cross–section model is compared with the phenomenological Bird and Svehla VHS model by simulating a high-enthalpy non-reacting molecular oxygen flow($U_\infty = 10000$ m/s) around an

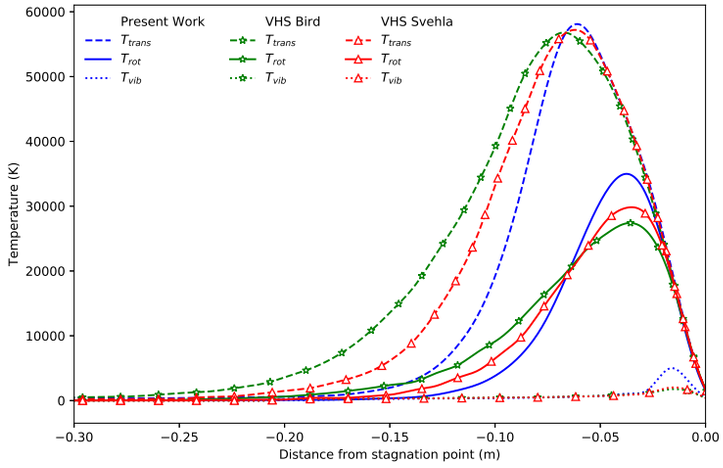

FIG. 9. Comparison of different modes of temperatures at the centreline for collision cross–section calculated in the present work with Bird and Svehla VHS model. Zero point refers to stagnation point on the cylinder.

infinite cylinder ($d = 304.8$ mm) at rarefied ambient conditions (Number density $= 1 \times 10^{20}$ m^{-3}, Temperature $= 200$ K) using the DSMC method. The cylinder surface temperature is fixed at 1000 K with diffuse gas–surface interaction model at full thermal accommodation. The time step chosen for the current simulation is 10^{-8} s. Larsen–Borgnakke (LB) model with constant relaxation parameters ($Z_{rot} = 5$ and $Z_{vib} = 50$) is employed to handle the inelastic collisions. At steady state, roughly 21×10^6 DSMC particles populate the 1000×1000 regular Cartesian grid in the 1m×1m domain. Figure 9 shows the centre–line plots of three modes of temperatures: translational, rotational and vibrational for the three sets of simulations. The effect of the collision cross–section model on temperature variation and on the shock structure is apparent. The higher collision cross–section estimated by the new model results in more number of collisions which in turn leads to increased probability of inelastic collisions. Higher rotational and vibrational temperatures is a direct consequence of higher degree of internal energy exchange in simulations employing the new model compared to those obtained in simulations with Svehla and Bird VHS models. The shock structure in the DSMC simulation employing the new collision cross–sections are less diffused than those noticed in the VHS model. The effect of vibrational level dependent collision cross–section model on flow physics in a realistic situation with chemical and ionization reactions will be taken up as a future work.

V. NONEQUILIBRIUM TRANSPORT COEFFICIENTS

Park[49] suggested a two-temperature model for calculating nonequilibrium chemical reaction rates. According to this two-temperature model, the translational and rotational modes of energy are assumed to be in full equilibrium with each other and can be replaced with a single trans-rotational temperature (T_{tr} or simply T). In addition, it is assumed that the vibrational and electronic modes of energies are in equilibrium with each other, leading to a single vibro-electronic temperature (T_{ve} or simply T_v). Park stated that, in the case of forward reactions, the temperatures supplied to the Arrhenius equation are the geometric mean of the trans-rotational and vibro-electronic temperatures. Several modifications to the temperature indices have been reported.[50] Further, a detailed discussion on the transport properties of the mixtures has also been presented.[47,51,52] However, the effect of the nonequilibrium state on the transport properties has not been thoroughly investigated. In the present work, it is clear that the collision cross-section depends on the vibrational energy. Thus, it is obvious that different combinations of trans-rotational and vibro-electronic temperatures will have a considerable effect on the transport properties, in particular, the viscosity coefficients. As vibrational level-dependent cross-sections are now available, it is possible to approximate the coefficient of viscosity in nonequilibrium conditions to the following relation, which is similar to Eq. (9):

$$\mu(T,T_v) = \frac{(5/8)(\pi m k T)^{1/2}}{(\frac{m}{4kT})^4 Q_v^{-1}[\sum_{v_1,v_2} exp(-\frac{E_{v_1}}{kT_v}) exp(-\frac{E_{v_2}}{kT_v}) \int_0^\infty c_r^7 \tfrac{2}{3} \sigma_T(v_1,v_2) exp(-\frac{m c_r^2}{4kT}) dc_r]} \tag{11}$$

where again c_r is the relative speed, T is the temperature, T_v is the vibrational temperature, E_{v_1} and E_{v_2} are the vibrational energies of the two molecules at v_1 and v_2 vibrational levels respectively, and Q_v is the partition function for the vibrational degree of freedom.

This formula is employed to calculate the coefficient of viscosity for various combinations of translational and vibrational temperature. The following analytical function is used to fit the data:

$$\mu(T,T_v) = a\left(\frac{T}{T_{ref}}\right)^{\omega}\left(\frac{T_v}{T_{ref}}\right)^{\omega_v} + b \tag{12}$$

where a, ω, ω_v, b, and T_{ref} are parameters. The parameters for various combinations of gases are listed in Table II. The maximum relative error for each of the fits is less than

0.1%.

TABLE II. Parameters for the analytical fit of nonequilibrium viscosities

	a	ω	ω_v	b	T_{ref}
N_2-N_2	4.4783e-05	0.6484	-0.0195	3.8948e-08	1000
O_2-O_2	5.6416e-05	0.6375	-0.0792	6.7929e-07	1000
N_2-O_2	4.3565e-05	0.6829	-0.0481	-1.6876e-07	1000

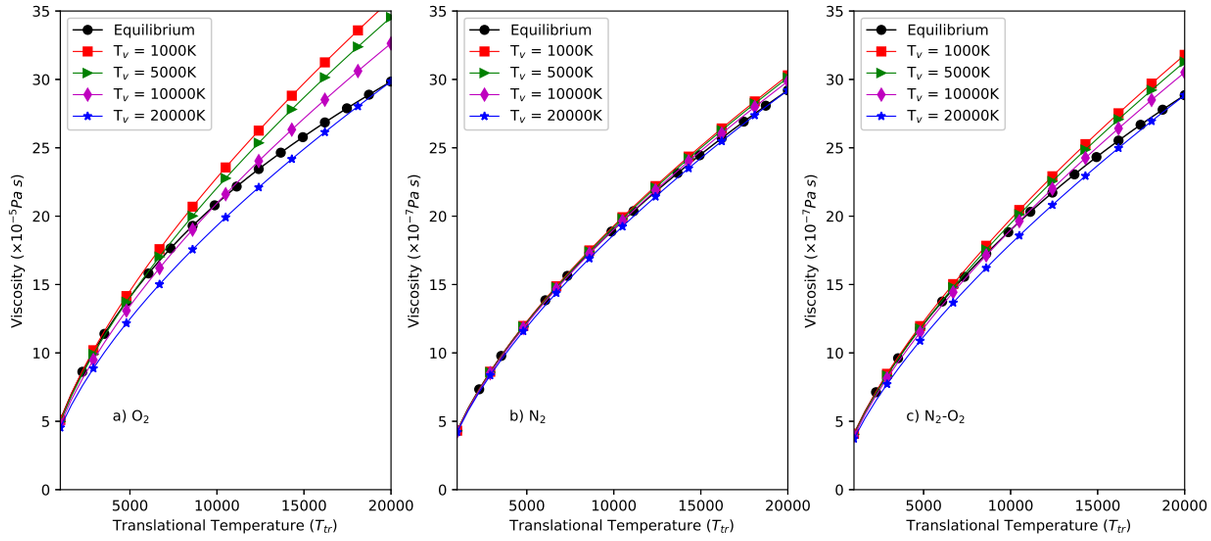

FIG. 10. Nonequilibrium effect of vibrational temperature on viscosity–temperature relation for (a) O_2-O_2 collisions, (b) N_2-N_2 collisions, and (c) N_2-O_2 collisions.

Figures 10(a)–10(c) show the effect of the varying vibrational temperature on viscosity–temperature relations for O_2-O_2, N_2-N_2, and N_2-O_2 systems, respectively. The viscosity–temperature relation in the equilibrium condition is also plotted along with the nonequilibrium viscosities to highlight the difference in the values. It is clear, especially at higher temperatures, that nonequilibrium conditions have a significant effect on the coefficient of viscosity. Additionally, when the conditions are further from equilibrium, there is a greater effect on the viscosity values. It is also noteworthy that the nonequilibrium effect is more pronounced in the case of the O_2-O_2 system than the N_2-N_2 system. From Fig. 10, it is evident that the effect of the vibrational level is stronger in the case of O_2-O_2 and N_2-O_2

collisions than for the N_2-N_2 collisions. The reason for this is likely to be the difference in the molecular structure of oxygen and nitrogen molecules. The equilibrium distances for different vibrational levels in the case of nitrogen molecules are smaller than those in oxygen molecules. Further, the extremities or turning points for the vibrating oxygen molecules are wider than those found in nitrogen molecules. As a result, the collision cross-sections for the nitrogen molecule at different vibrational levels, as shown in Fig. 7(b), are more compact than those observed for the oxygen molecule (shown in Fig. 7).

At higher altitudes, the nonequilibrium degree is very high. Thus, the temperatures corresponding to different modes of energy are different, and the distribution of populations in different energy levels does not correspond to an equilibrium one. The formulation provided in the present work can be used to calculate the transport properties in situations with nonequilibrium energy distributions. In our previous work, the vibrational energy distribution in the shock front and at the stagnation point was analyzed.[53] The translational, rotational, vibrational, trans-rotational, and total temperatures in the shock front for reacting oxygen flow over a cylinder at a re-entry speed of 5000 m/s are 14 000 K, 6700 K, 1065 K, 11 080 K, and 9820 K, respectively. Five separate cases are considered for calculating the local viscosity in the shock front. A single-temperature viscosity model employing either the translational (T_t), trans-rotational (T_{tr}), or total (T_{tot}) temperature is used. In addition, the two-temperature model detailed in the present work, employing the trans-rotational and vibrational temperatures, is used. Finally, a nonequilibrium model employing the actual vibrational and kinetic energy distributions, instead of an equilibrium distribution for the vibrational and translational temperatures, is used to calculate the viscosity. The results are presented in Table III. The difference in the viscosity calculated using the single-temperature model employing the translational temperature and the two-temperature model presented in this work is around 12%. Further, the difference in the viscosity calculated using the two-temperature model assuming an equilibrium distribution for the vibrational and kinetic energy with the nonequilibrium model is around 3%. It is clear that the difference in the viscosity values given by the different models is considerable, thus highlighting the need to choose the transport coefficient models and parameters more carefully. At higher re-entry speeds, the distribution of the vibrational energies will further diverge from the equilibrium distribution, making the difference in the viscosities calculated using the two-temperature model and the nonequilibrium model more prominent.

TABLE III. Comparison of viscosities calculated using different models in the shock front for re-entry flow ($U_\infty = 5000$ m/s)

Model	Viscosity ($\times 10^{-5}$ $Pa\ \ s$)
Single Temperature ($T = T_t = 14\,000$ K)	24.9472
Single Temperature ($T = T_{tr} = 11\,080$ K)	22.1128
Single Temperature ($T = T_{tot} = 9820$ K)	20.7396
Two Temperature ($T_{tr} = 14\,000$ K and $T_{vib} = 1065$)	28.4018
Nonequilibrium Model	27.4876

In the case of re-entry flows, highly nonequilibrium conditions are encountered, and hence it is important to include the nonequilibrium effects on the transport coefficients. Generally, the vibrational temperature is much lower than the trans-rotational temperature because of the higher relaxation time for vibrational energy distribution. The figures suggest that the viscosity values employed in traditional codes underpredict the viscous effect. This might have significant ramifications for the boundary layers and, subsequently, the surface properties. As stated in the previous section, the theoretical limitations of calculating collision cross-sections that are a function of vibrational level affects the calculation of nonequilibrium transport properties. Hence, the present work employs first-order approximations to calculate the transport properties. Higher-order approximations of the transport properties based on nonlinear theories will be employed in the future.

VI. CONCLUSION

Atom–atom, atom–molecule, and molecule–molecule collision cross-sections are extremely important for several applications. This work has examined the calculation of the collision cross-sections for several collision partners encountered in air chemistry. Our investigations established that the rotational levels have a negligible effect on the collision cross-section of diatomic molecule interactions. However, the same cannot be concluded for the vibrational levels. The collision cross-sections for higher vibrational levels are significantly higher than those calculated at the zeroth vibrational level. Additionally, the collision cross-sections cal-

culated in the present work are appreciably different from the VHS cross-sections employing different sets of parameters. In highly nonequilibrium simulation conditions, the effect of the vibrational levels on the collision cross-section can be vital. This factor is often neglected by widely used phenomenological models. In the case of re-entry flows, the vibrational levels in the vicinity of the shock have a nonequilibrium distribution. The population of the diatomic molecules in lower vibrational levels is higher than the equilibrium distribution population at the given vibrational temperature. At lower vibrational levels, the collision cross-sections calculated using the present method are smaller than the values predicted by the VHS models. This directly affects the collision rate and the reaction probability in cases where the energy of the collision is higher than the activation energy. Additionally, the scattering angle distribution derived in the present work can be used to model collisions in a better manner for DSMC-like methods. For continuum-based solvers, the effect of nonequilibrium conditions on the coefficient of viscosity was examined. This new transport property model will have a profound effect on the physics of re-entry flows.

VII. SUPPLEMENTARY MATERIAL

The fitting parameters for collision cross-section for N_2-N, O_2-O, N_2-N_2, O_2-O_2 and N_2-O_2 collision pairs are tabulated in the supplementary material.

VIII. ACKNOWLEDGMENTS

T. K. M. and R. S. M. acknowledge the support from the National Research Foundation of Korea funded by the Ministry of Education, Science and Technology (NRF 2017-R1A2B2007634 and 2017-M1A3A3A03016312), South Korea.

REFERENCES

[1]S. K. Stefanov, Physics of Fluids **31**, 067104 (2019), https://doi.org/10.1063/1.5099042.

[2]R. S. Myong, A. Karchani, and O. Ejtehadi, Physics of Fluids **31**, 066101 (2019), https://doi.org/10.1063/1.5093746.

[3]G. A. Bird, Progress in Astronautics and Aeronautics **74**, 239 (1981).

[4]K. Koura and H. Matsumoto, Physics of Fluids A: Fluid Dynamics **3**, 2459 (1991).

[5]H. A. Hassan and D. B. Hash, Physics of Fluids A: Fluid Dynamics **5**, 738 (1993), https://doi.org/10.1063/1.858656.

[6]J. Fan, Physics of Fluids **14**, 4399 (2002), https://doi.org/10.1063/1.1521123.

[7]H. Matsumoto and K. Koura, Physics of Fluids A: Fluid Dynamics **3**, 3038 (1991).

[8]A. Venkattraman and A. Alexeenko, in *42nd AIAA Thermophysics Conference*, p. 3313.

[9]A. Venkattraman and A. Alexeenko, Physics of Fluids **24**, 027101 (2012).

[10]F. Sharipov and J. L. Strapasson, Physics of Fluids **24**, 011703 (2012).

[11]F. Sharipov and F. C. Dias, Computers & Fluids **150**, 115 (2017).

[12]N. Parsons, D. A. Levin, A. C. T. van Duin, and T. Zhu, The Journal of Chemical Physics **141**, 234307 (2014), http://dx.doi.org/10.1063/1.4903782.

[13]J. D. Bender, P. Valentini, I. Nompelis, Y. Paukku, Z. Varga, D. G. Truhlar, T. Schwartzentruber, and G. V. Candler, The Journal of Chemical Physics **143**, 054304 (2015).

[14]M. Kulakhmetov, M. Gallis, and A. Alexeenko, The Journal of Chemical Physics **144**, 174302 (2016), http://dx.doi.org/10.1063/1.4947590.

[15]D. A. Andrienko and I. D. Boyd, The Journal of Chemical Physics **144**, 104301 (2016), http://dx.doi.org/10.1063/1.4943114.

[16]W. Lin, R. Meana-Pañeda, Z. Varga, and D. G. Truhlar, The Journal of Chemical Physics **144**, 234314 (2016).

[17]H. Luo, M. Kulakhmetov, and A. Alexeenko, The Journal of Chemical Physics **146**, 074303 (2017).

[18]J. G. Kim and I. D. Boyd, Physics of Fluids **26**, 012006 (2014).

[19]E. V. Kustova and G. M. Kremer, in *AIP Conference Proceedings*, Vol. 1786 (2016) p. 070002.

[20]H. Luo, I. B. Sebastião, A. A. Alexeenko, and S. O. Macheret, Physical Review Fluids **3**, 113401 (2018).

[21]H. Luo, A. A. Alexeenko, and S. O. Macheret, Physics of Fluids **31**, 087105 (2019), https://doi.org/10.1063/1.5110162.

[22]T. K. Mankodi, U. V. Bhandarkar, and B. P. Puranik, The Journal of Chemical Physics **146**, 204307 (2017), http://dx.doi.org/10.1063/1.4983813.

[23]T. K. Mankodi, U. V. Bhandarkar, and B. P. Puranik, The Journal of Chemical Physics **148**, 074305 (2018).

[24]T. K. Mankodi and R. S. Myong, Physics of Fluids **31**, 106102 (2019).

[25]T. K. Mankodi and R. S. Myong, Physics of Fluids **32**, 019901 (2020), https://doi.org/10.1063/1.5142303.

[26]J. H. Chae, T. K. Mankodi, S. M. Choi, and R. S. Myong, International Journal of Aeronautical and Space Sciences (2019), 10.1007/s42405-019-00243-9.

[27]R. M. Berns and A. van der Avoird, The Journal of Chemical Physics **72**, 6107 (1980).

[28]V. Aquilanti, M. Bartolomei, D. Cappelletti, E. Carmona-Novillo, and F. Pirani, The Journal of Chemical Physics **117**, 615 (2002).

[29]R. Hernández-Lamoneda, M. Bartolomei, M. I. Hernández, J. Campos-Martínez, and F. Dayou, The Journal of Physical Chemistry A **109**, 11587 (2005), pMID: 16354051, http://dx.doi.org/10.1021/jp053728g.

[30]A. Scemama, M. Caffarel, and A. Ramírez-Solís, The Journal of Physical Chemistry A **113**, 9014 (2009), pMID: 19719306, http://dx.doi.org/10.1021/jp902028g.

[31]Y. Paukku, K. R. Yang, Z. Varga, G. Song, J. D. Bender, and D. G. Truhlar, The Journal of Chemical Physics **147**, 034301 (2017).

[32]Y. Paukku, Z. Varga, and D. G. Truhlar, The Journal of Chemical Physics **148**, 124314 (2018).

[33]Y. Paukku, K. R. Yang, Z. Varga, and D. G. Truhlar, The Journal of Chemical Physics **139**, 044309 (2013), http://dx.doi.org/10.1063/1.4811653.

[34]Z. Varga, R. Meana-Pañeda, G. Song, Y. Paukku, and D. G. Truhlar, The Journal of Chemical Physics **144**, 024310 (2016), http://dx.doi.org/10.1063/1.4939008.

[35]R. J. Duchovic, Y. L. Volobuev, G. C. Lynch, D. G. Truhlar, T. C. Allison, A. F. Wagner, B. C. Garrett, and J. C. Corchado, Computer Physics Communications **2**, 169 (2002).

[36]M. Karplus, R. N. Porter, and R. D. Sharma, The Journal of Chemical Physics **43**, 3259 (1965).

[37]D. G. Truhlar and J. T. Muckerman, "Reactive scattering cross sections iii: Quasiclassical and semiclassical methods," in *Atom - Molecule Collision Theory: A Guide for the Experimentalist*, edited by R. B. Bernstein (Springer US, Boston, MA, 1979) pp. 505–566.

[38]W. G. Vincenti and C. H. Kruger, *Introduction to physical gas dynamics* (Wiley, New York, 1965).

[39]G. A. Bird, *Molecular gas dynamics and the direct simulation of gas flows* (Clarendon, 1994).

[40]R. A. Svehla, Estimated Viscosities and Thermal Conductivities of Gases at High Temperature, NASA Technical Report, R-132 (1962).

[41]T. Ozawa, *Improved chemistry models for Dsmc simulations of ionized rarefied hypersonic flows* (PhD. Thesis, The Pennsylvania State University).

[42]R. S. Myong, Journal of Computational Physics **195**, 655 (2004).

[43]S. Singh, A. Karchani, and R. S. Myong, Physics of Fluids **30**, 016109 (2018).

[44]S. Bhola and T. K. Sengupta, Physics of Fluids **31**, 096101 (2019), https://doi.org/10.1063/1.5099206.

[45]S. Singh, A. Karchani, K. Sharma, and R. S. Myong, Physics of Fluids **32** (2020), https://doi.org/10.1063/1.5133079.

[46]A. Boushehri, J. Bzowski, J. Kestin, and E. Mason, Journal of physical and chemical reference data **16**, 445 (1987).

[47]C. Wilke, The Journal of Chemical Physics **18**, 517 (1950).

[48]F. G. Blottner, M. Johnson, and M. Ellis, "Chemically reacting viscous flow program for multi-component gas mixtures." Tech. Rep. (Sandia Labs., Albuquerque, N. Mex., 1971).

[49]C. Park, *Nonequilibrium Hypersonic Aerothermodynamics* (Wiley, New York, 1990).

[50]G. V. Candler and I. Nompelis, "Computational fluid dynamics for atmospheric entry," Tech. Rep. (Minnesota Univ. Minneapolis Dept. of Aerospace Engineering and Mechanics, 2009).

[51]B. Armaly and K. Sutton, in *15th Thermophysics Conference, Los Angeles, USA* (1980) p. 1495.

[52]G. E. Palmer and M. J. Wright, Journal of Thermophysics and Heat Transfer **17**, 232 (2003).

[53]T. Mankodi, U. Bhandarkar, and B. Puranik, The Journal of Chemical Physics **148**, 144305 (2018).

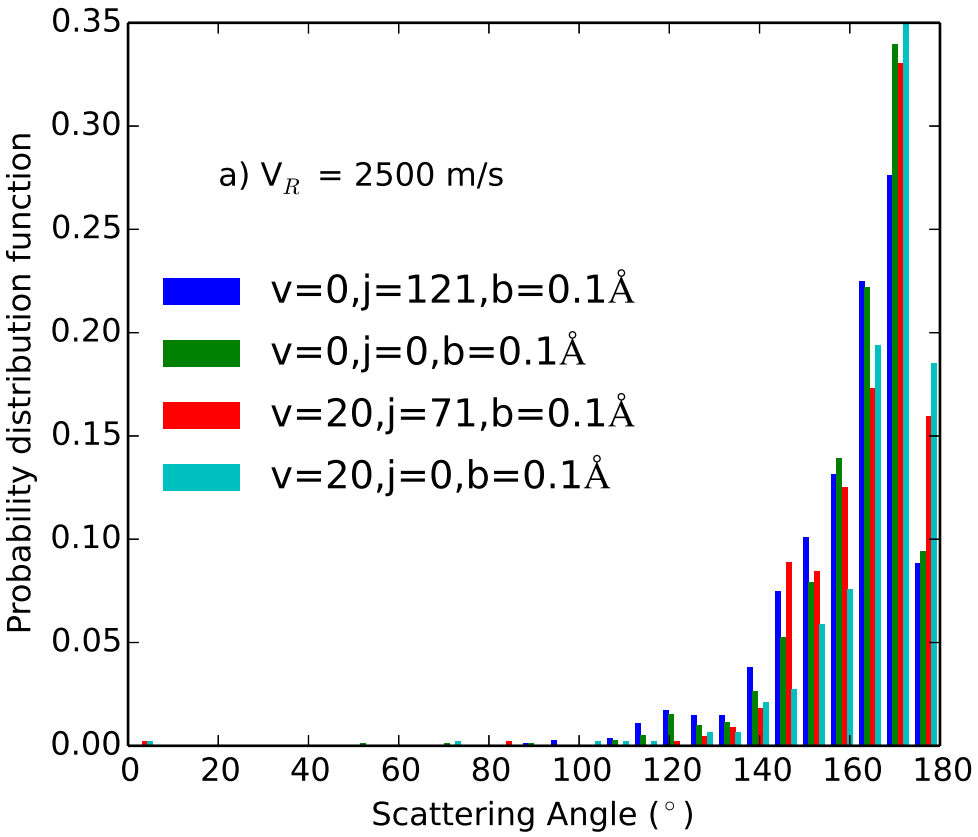
a) V_R = 2500 m/s
v=0,j=121,b=0.1Å
v=0,j=0,b=0.1Å
v=20,j=71,b=0.1Å
v=20,j=0,b=0.1Å
Probability distribution function
Scattering Angle (°)

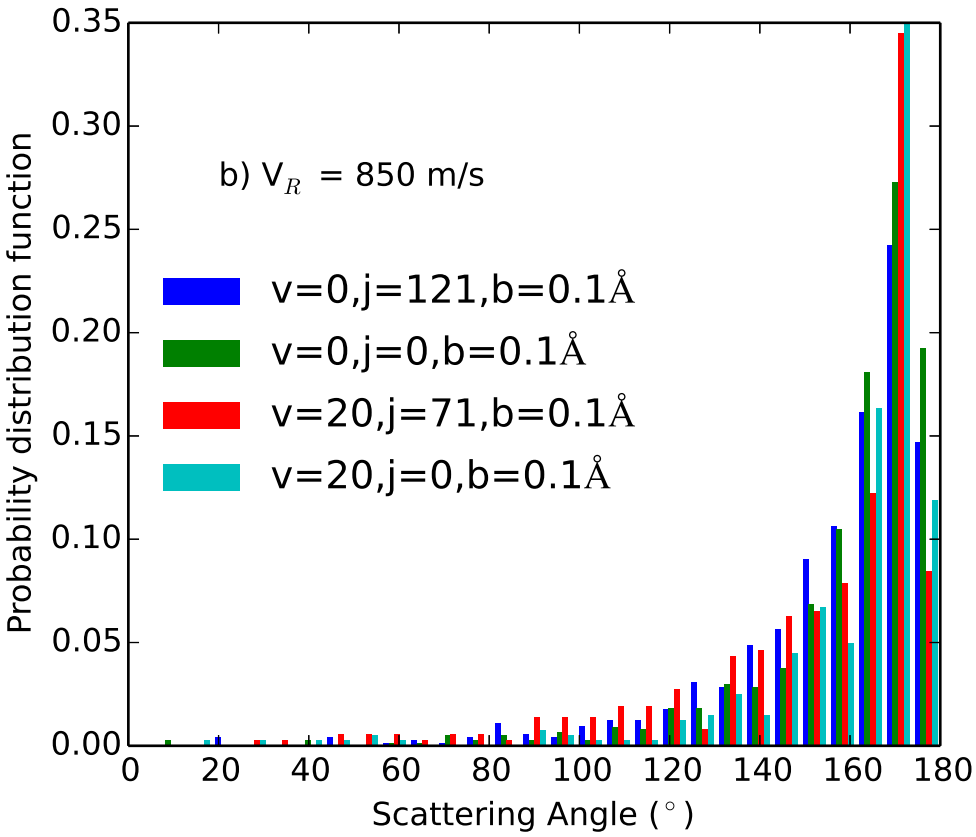
b) V_R = 850 m/s
v=0,j=121,b=0.1Å
v=0,j=0,b=0.1Å
v=20,j=71,b=0.1Å
v=20,j=0,b=0.1Å
Probability distribution function
Scattering Angle (°)

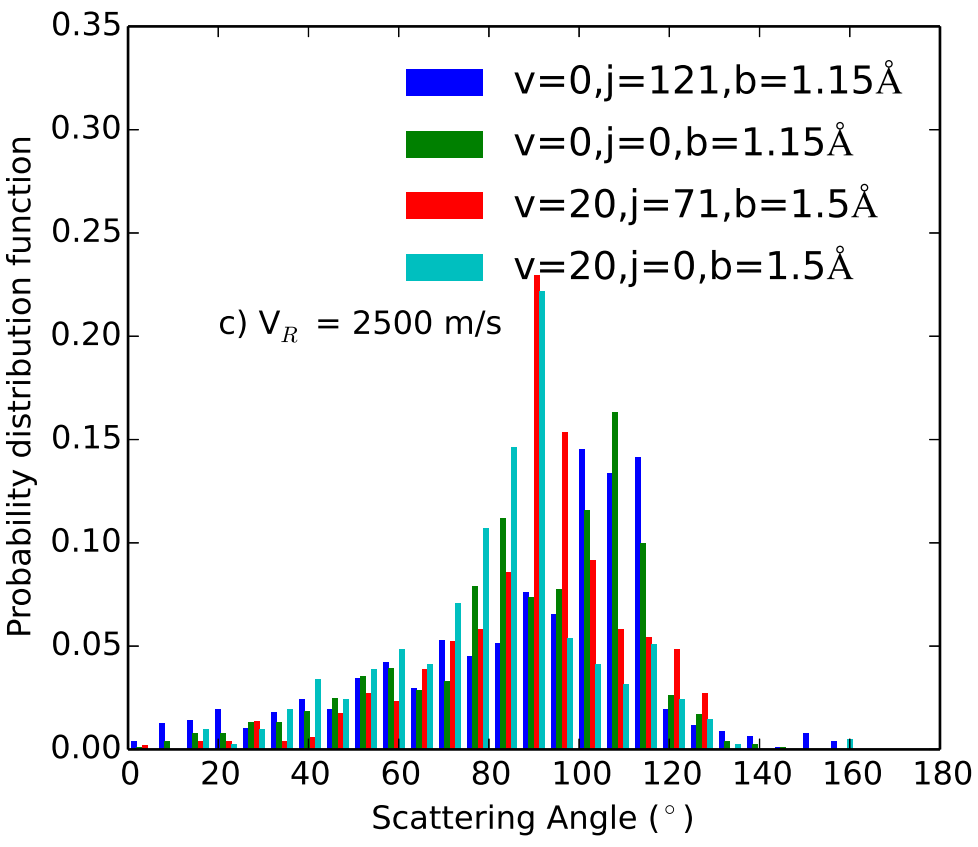
c) V_R = 2500 m/s
v=0,j=121,b=1.15Å
v=0,j=0,b=1.15Å
v=20,j=71,b=1.5Å
v=20,j=0,b=1.5Å
Probability distribution function
Scattering Angle (°)

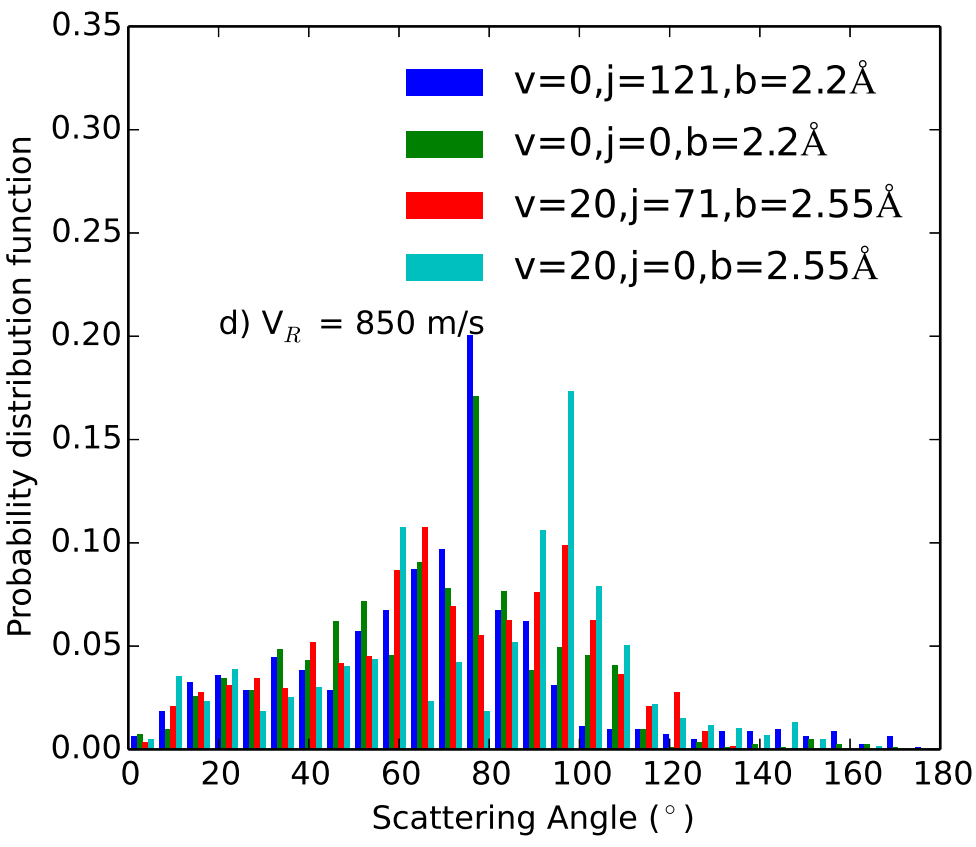
d) V_R = 850 m/s
v=0,j=121,b=2.2Å
v=0,j=0,b=2.2Å
v=20,j=71,b=2.55Å
v=20,j=0,b=2.55Å
Probability distribution function
Scattering Angle (°)

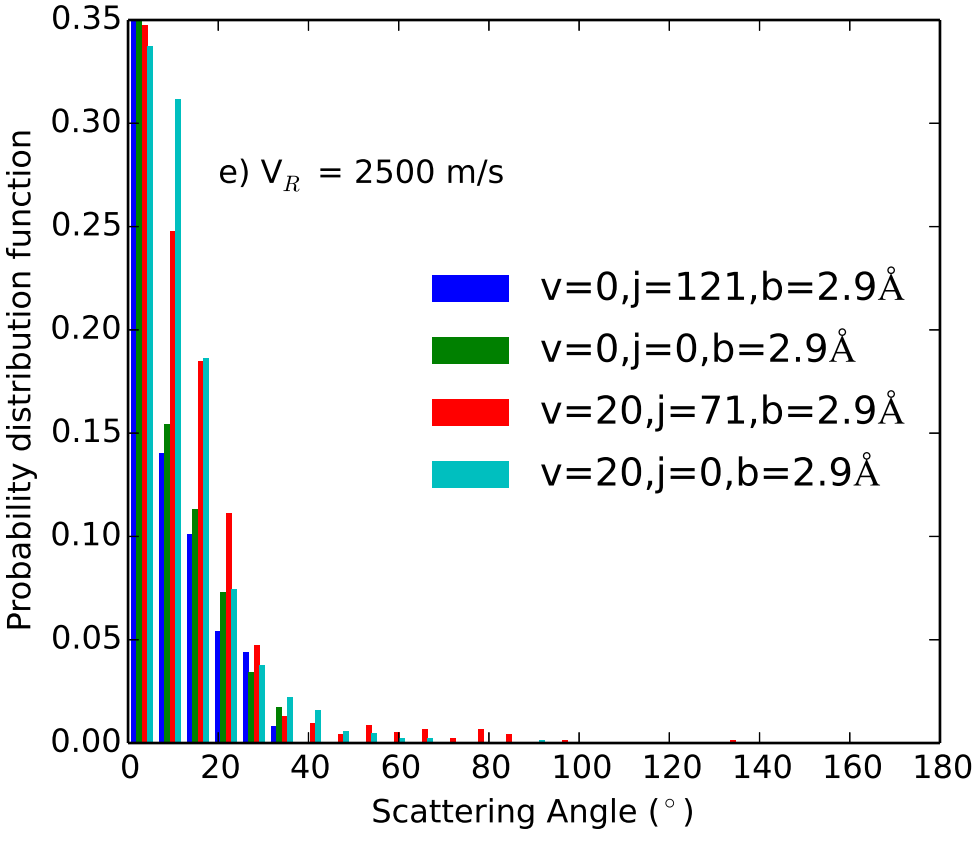
e) V_R = 2500 m/s
v=0,j=121,b=2.9Å
v=0,j=0,b=2.9Å
v=20,j=71,b=2.9Å
v=20,j=0,b=2.9Å
Probability distribution function
Scattering Angle (°)

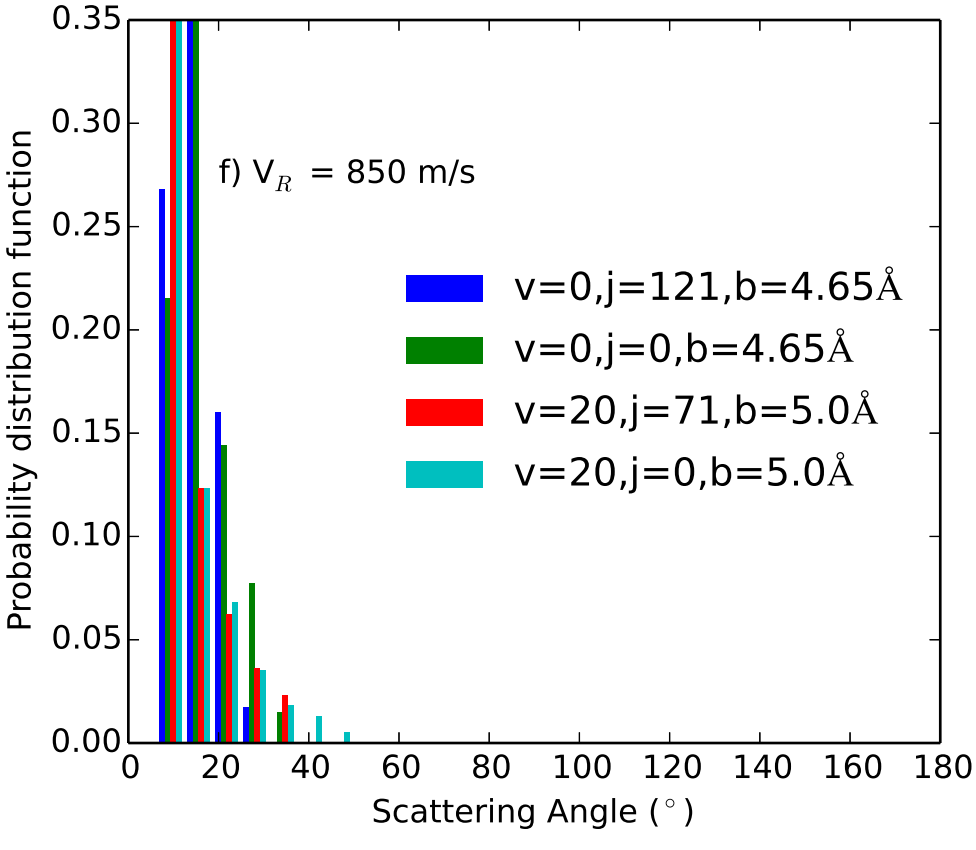
f) V_R = 850 m/s
v=0,j=121,b=4.65Å
v=0,j=0,b=4.65Å
v=20,j=71,b=5.0Å
v=20,j=0,b=5.0Å
Probability distribution function
Scattering Angle (°)

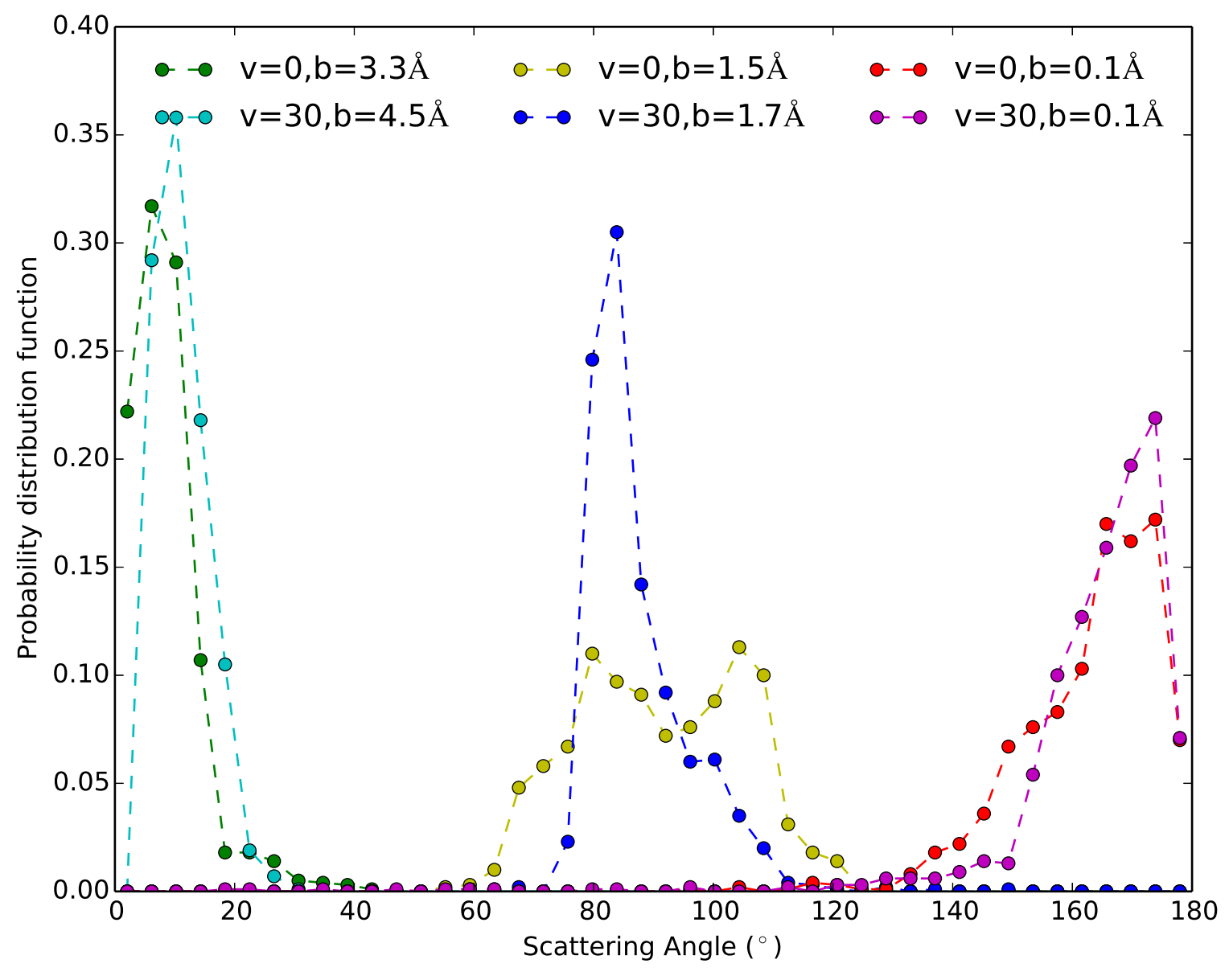
v=0,b=3.3Å
v=0,b=1.5Å
v=0,b=0.1Å
v=30,b=4.5Å
v=30,b=1.7Å
v=30,b=0.1Å
Probability distribution function
Scattering Angle (°)
0.00
0.05
0.10
0.15
0.20
0.25
0.30
0.35
0.40
0
20
40
60
80
100
120
140
160
180

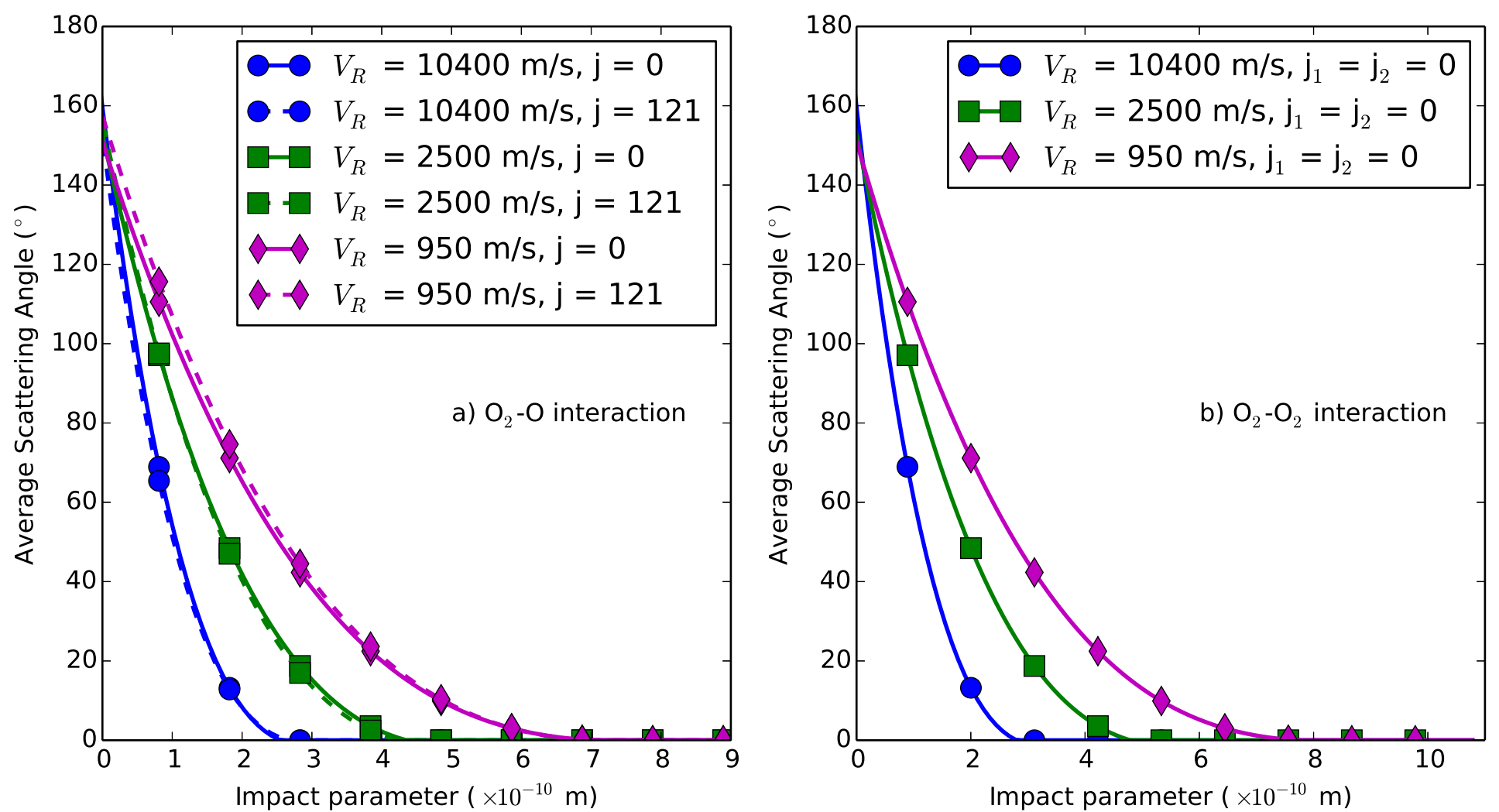
V_R = 10400 m/s, j = 0
V_R = 10400 m/s, j = 121
V_R = 2500 m/s, j = 0
V_R = 2500 m/s, j = 121
V_R = 950 m/s, j = 0
V_R = 950 m/s, j = 121
a) O_2-O interaction
Average Scattering Angle (°)
Impact parameter ($\times 10^{-10}$ m)
V_R = 10400 m/s, j_1 = j_2 = 0
V_R = 2500 m/s, j_1 = j_2 = 0
V_R = 950 m/s, j_1 = j_2 = 0
b) O_2-O_2 interaction
Average Scattering Angle (°)
Impact parameter ($\times 10^{-10}$ m)

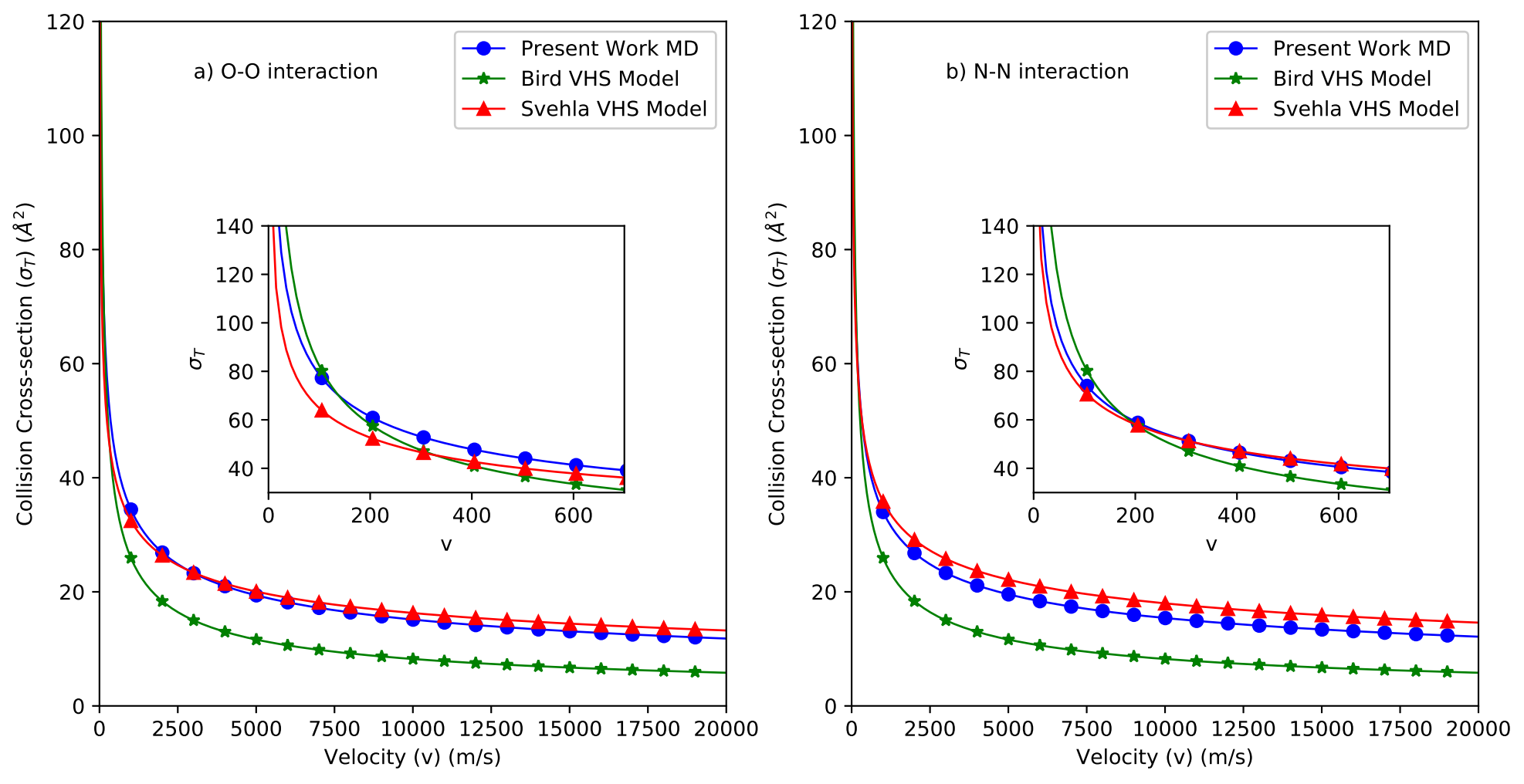
a) O-O interaction
Present Work MD
Bird VHS Model
Svehla VHS Model
Collision Cross-section (σ_T) ($\AA^2$)
Velocity (v) (m/s)
σ_T
v
b) N-N interaction
Present Work MD
Bird VHS Model
Svehla VHS Model
Collision Cross-section (σ_T) ($\AA^2$)
Velocity (v) (m/s)
σ_T
v

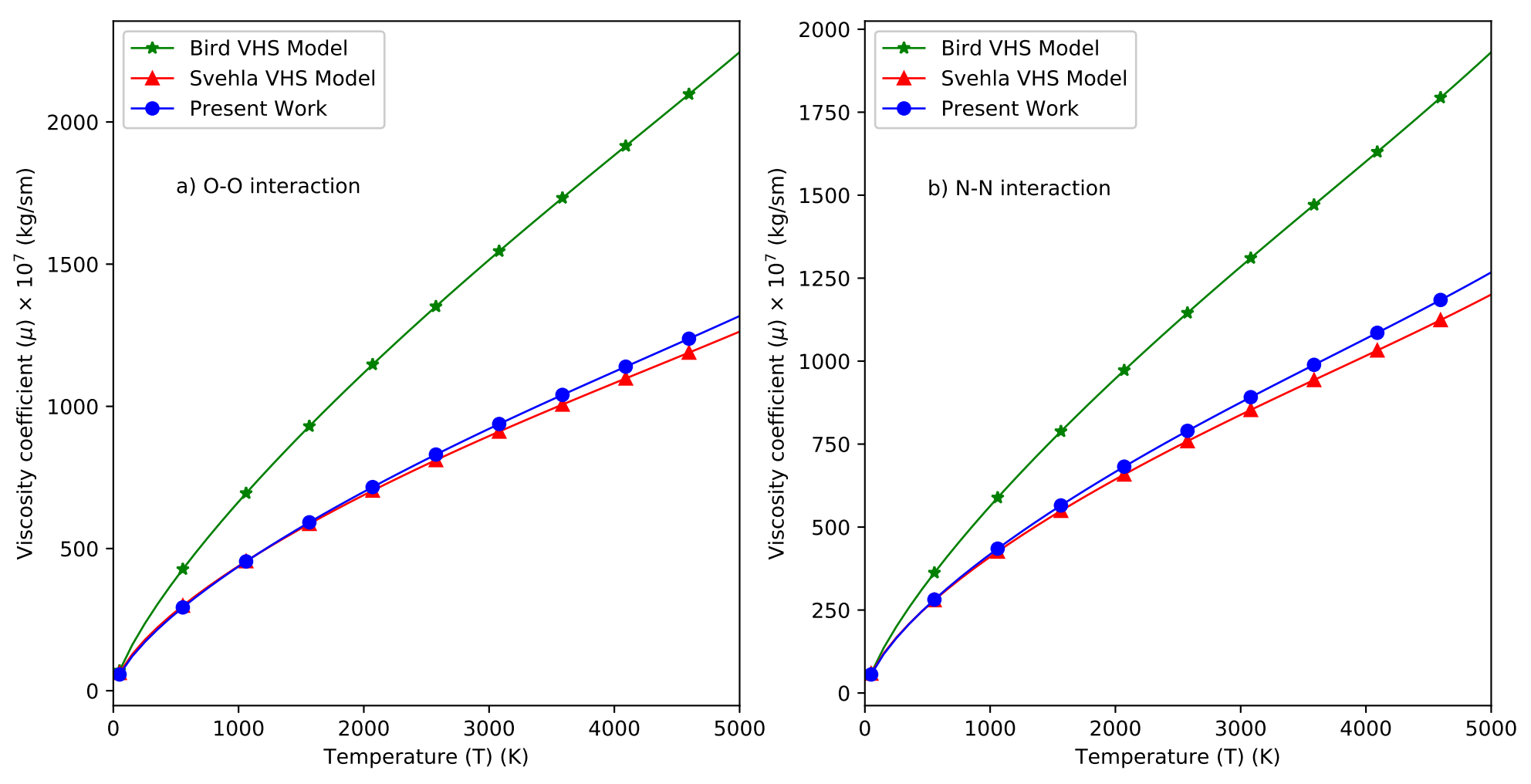
Bird VHS Model
Svehla VHS Model
Present Work
a) O-O interaction
Viscosity coefficient (μ) × 10^7 (kg/sm)
Temperature (T) (K)
0
500
1000
1500
2000
0
1000
2000
3000
4000
5000
Bird VHS Model
Svehla VHS Model
Present Work
b) N-N interaction
Viscosity coefficient (μ) × 10^7 (kg/sm)
Temperature (T) (K)
0
250
500
750
1000
1250
1500
1750
2000
0
1000
2000
3000
4000
5000

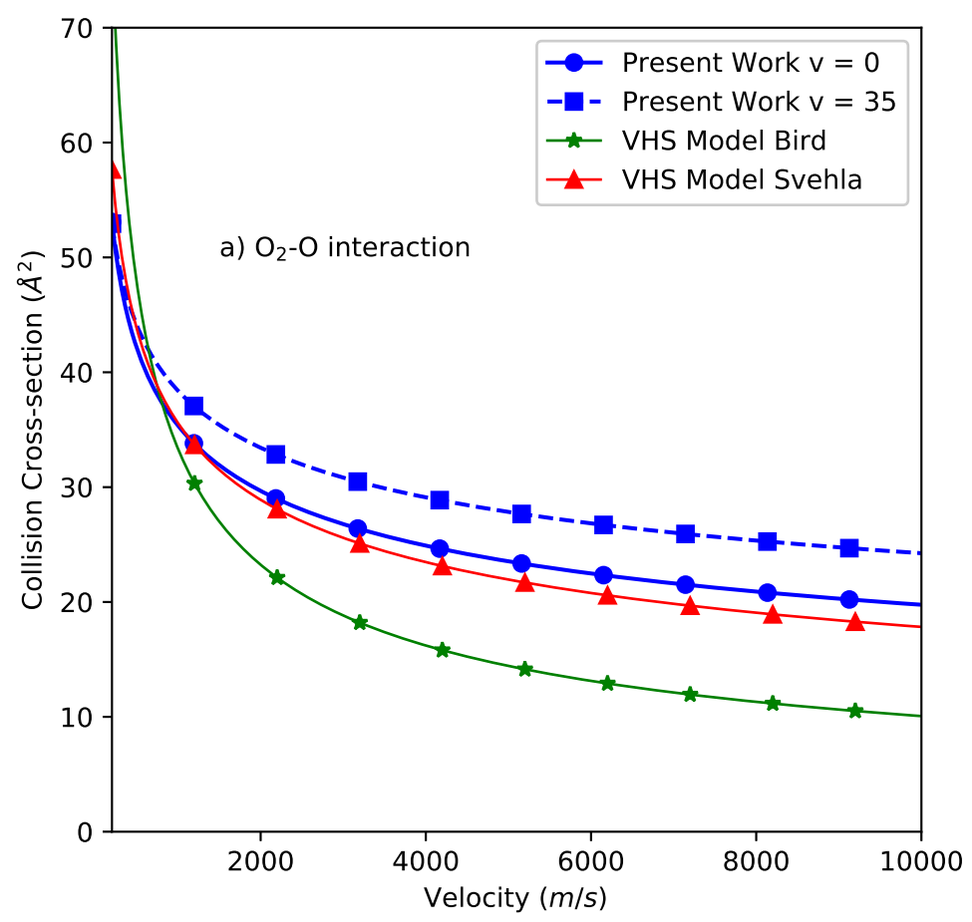
Present Work v = 0
Present Work v = 35
VHS Model Bird
VHS Model Svehla
a) O_2-O interaction
Collision Cross-section ($Å^2$)
Velocity (m/s)
0
10
20
30
40
50
60
70
2000
4000
6000
8000
10000

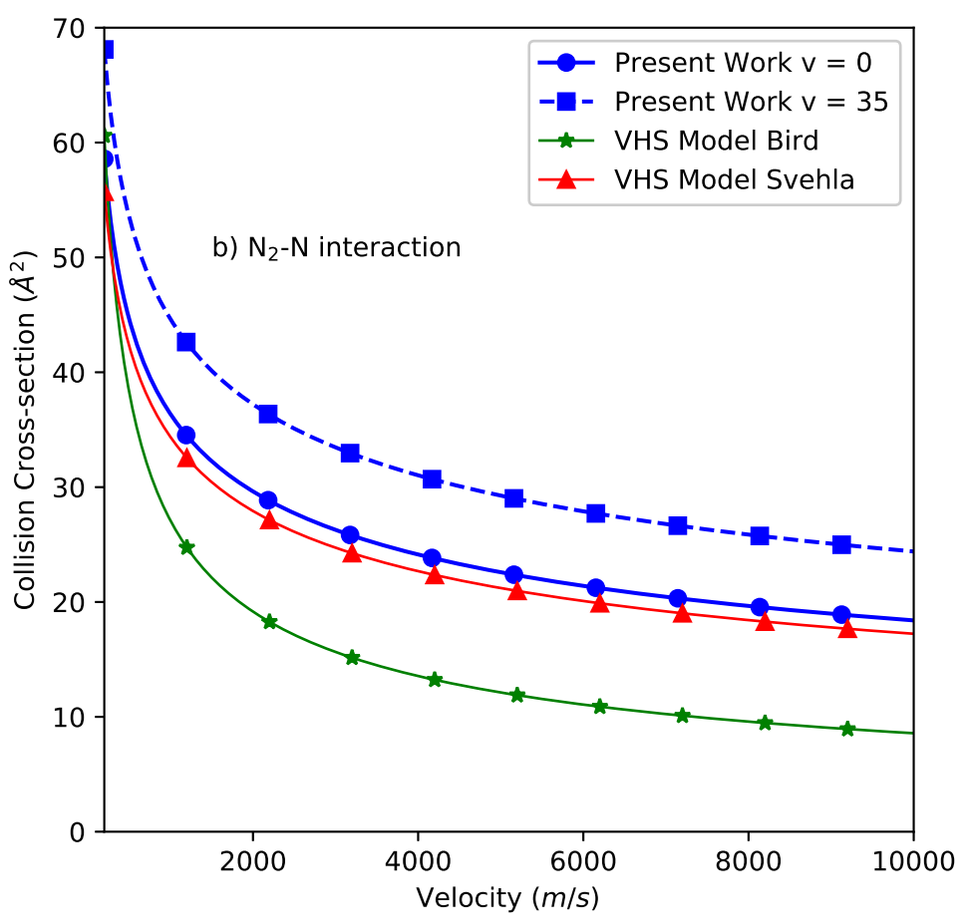
Present Work v = 0
Present Work v = 35
VHS Model Bird
VHS Model Svehla
b) N_2-N interaction
Collision Cross-section ($Å^2$)
Velocity (m/s)
0
10
20
30
40
50
60
70
2000
4000
6000
8000
10000

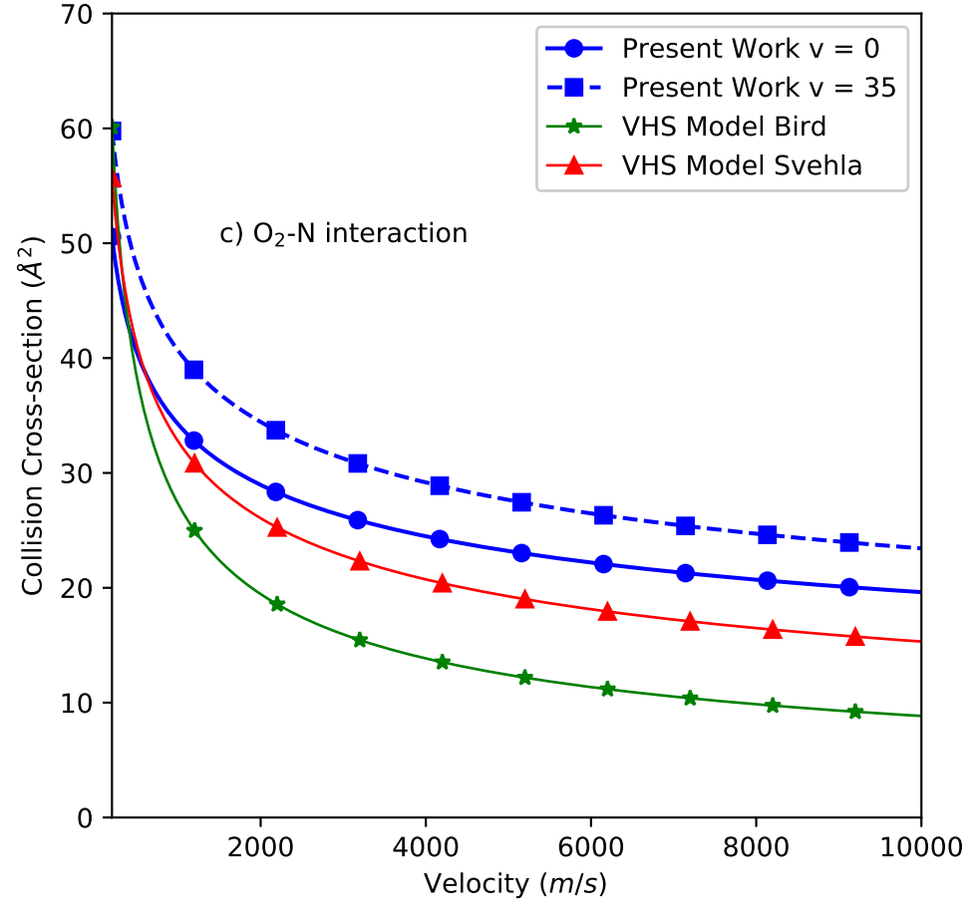
Present Work v = 0
Present Work v = 35
VHS Model Bird
VHS Model Svehla
c) O_2-N interaction
Collision Cross-section ($Å^2$)
Velocity (m/s)
0
10
20
30
40
50
60
70
2000
4000
6000
8000
10000

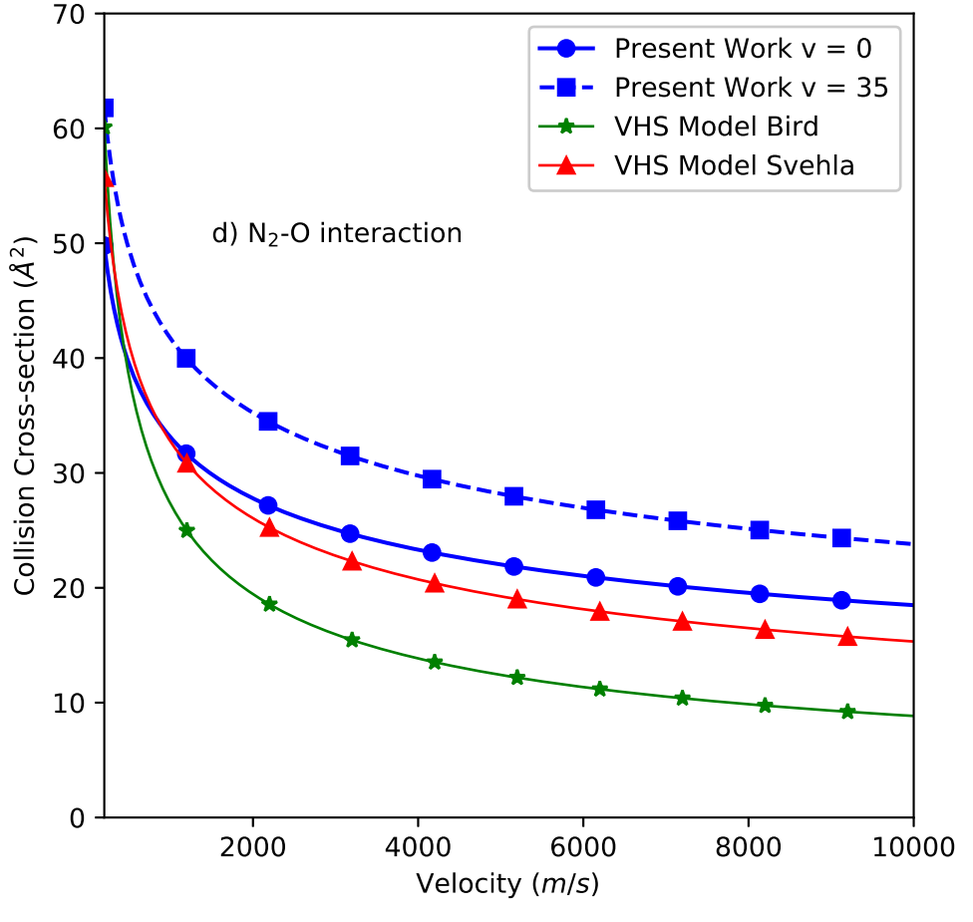
Present Work v = 0
Present Work v = 35
VHS Model Bird
VHS Model Svehla
d) N_2-O interaction
Collision Cross-section ($Å^2$)
Velocity (m/s)
0
10
20
30
40
50
60
70
2000
4000
6000
8000
10000

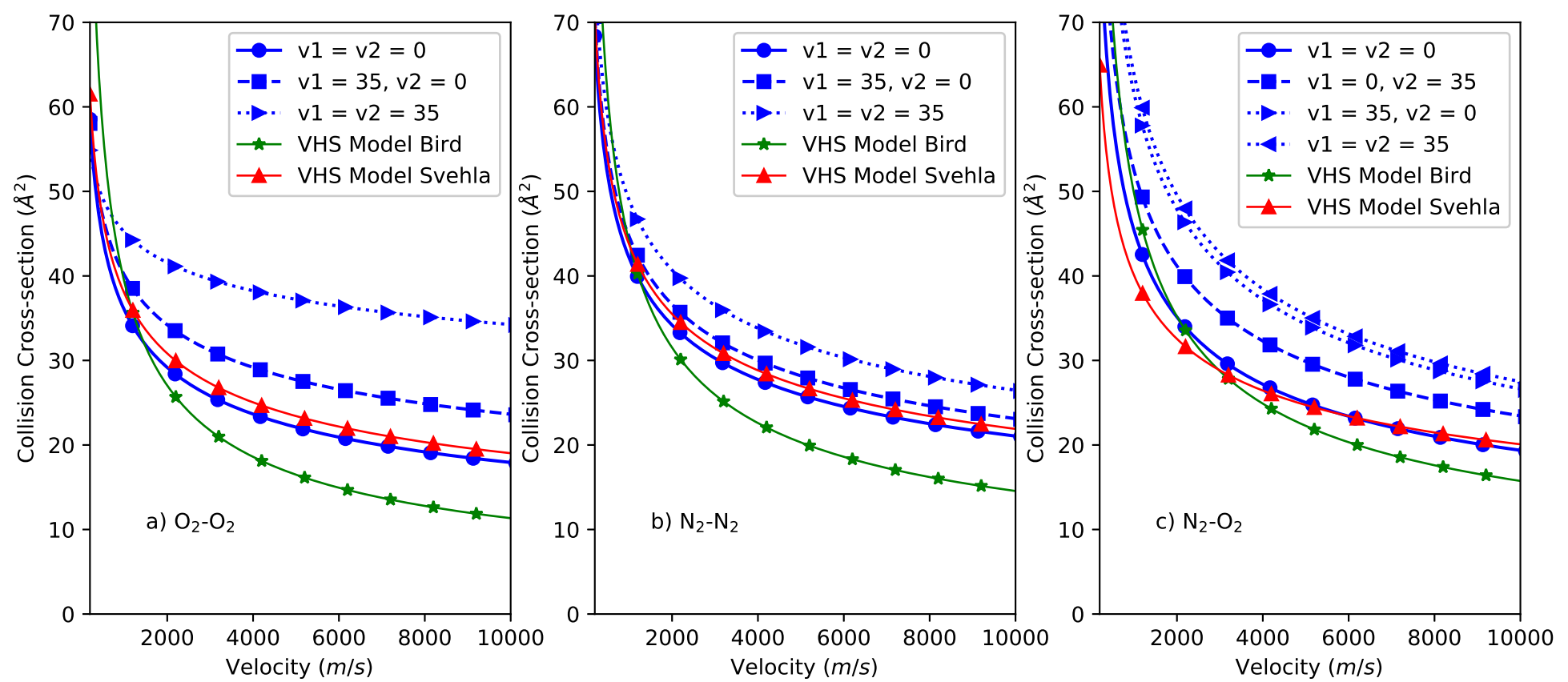
v1 = v2 = 0
v1 = 35, v2 = 0
v1 = v2 = 35
VHS Model Bird
VHS Model Svehla
Collision Cross-section ($Å^2$)
Velocity (m/s)
a) O_2-O_2
b) N_2-N_2
v1 = 0, v2 = 35
c) N_2-O_2

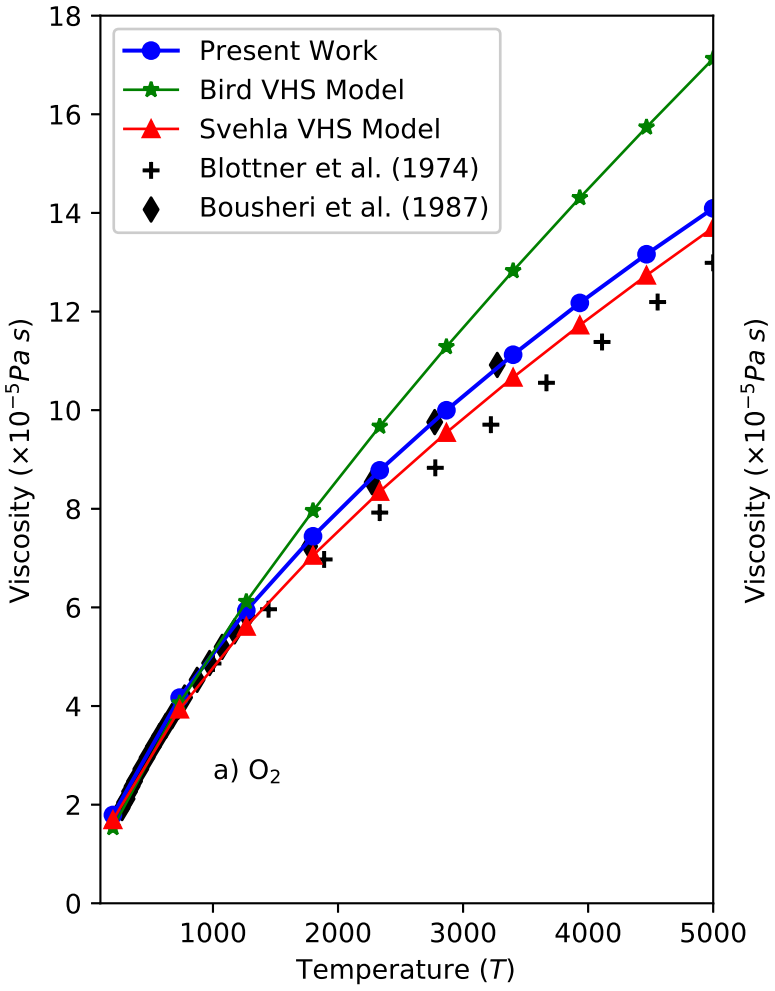
Present Work
Bird VHS Model
Svehla VHS Model
Blottner et al. (1974)
Bousheri et al. (1987)
Viscosity ($\times 10^{-5} Pa\ s$)
Temperature (T)
a) O_2

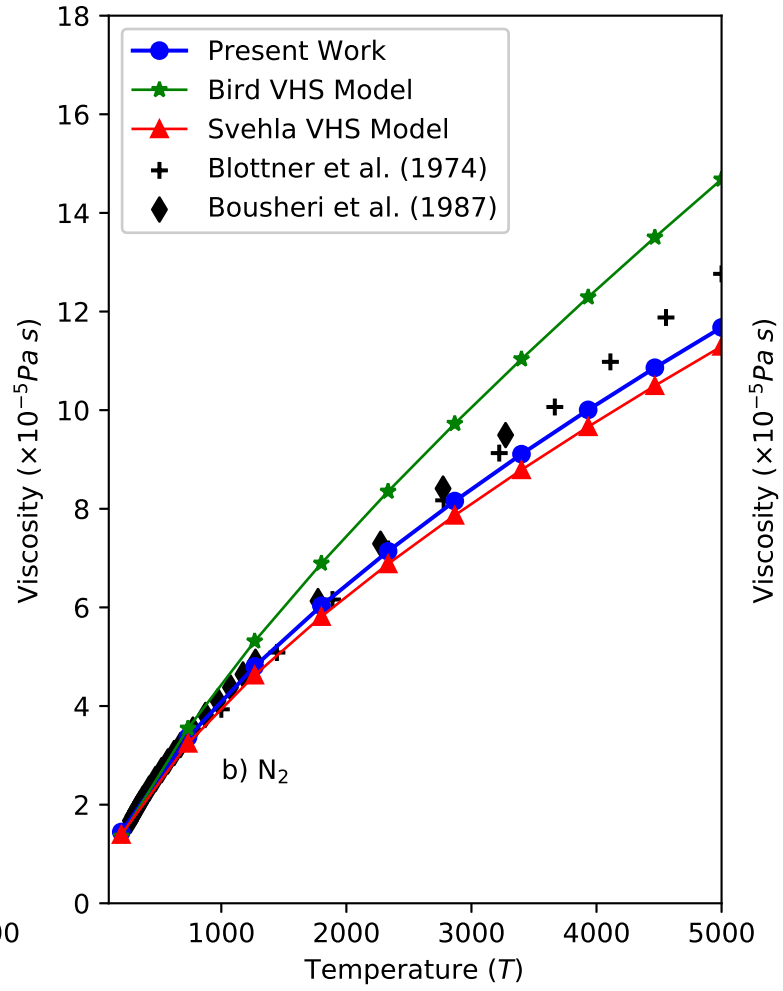
Present Work
Bird VHS Model
Svehla VHS Model
Blottner et al. (1974)
Bousheri et al. (1987)
Viscosity ($\times 10^{-5} Pa\ s$)
Temperature (T)
b) N_2

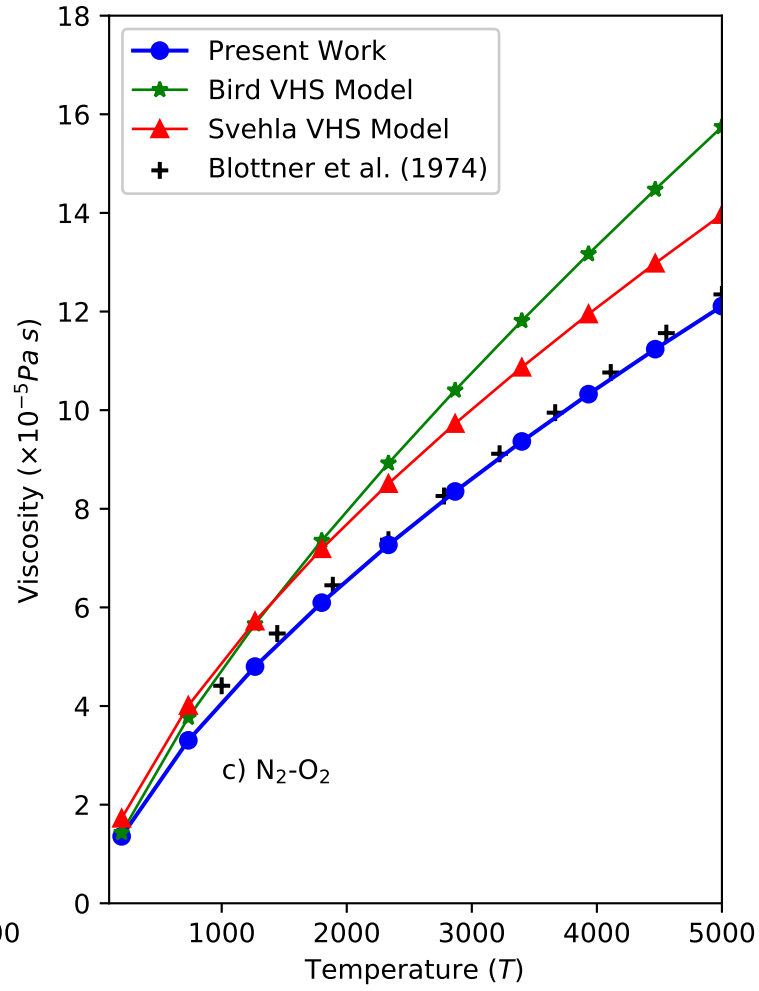
Present Work
Bird VHS Model
Svehla VHS Model
Blottner et al. (1974)
Viscosity ($\times 10^{-5} Pa\ s$)
Temperature (T)
c) N_2-O_2

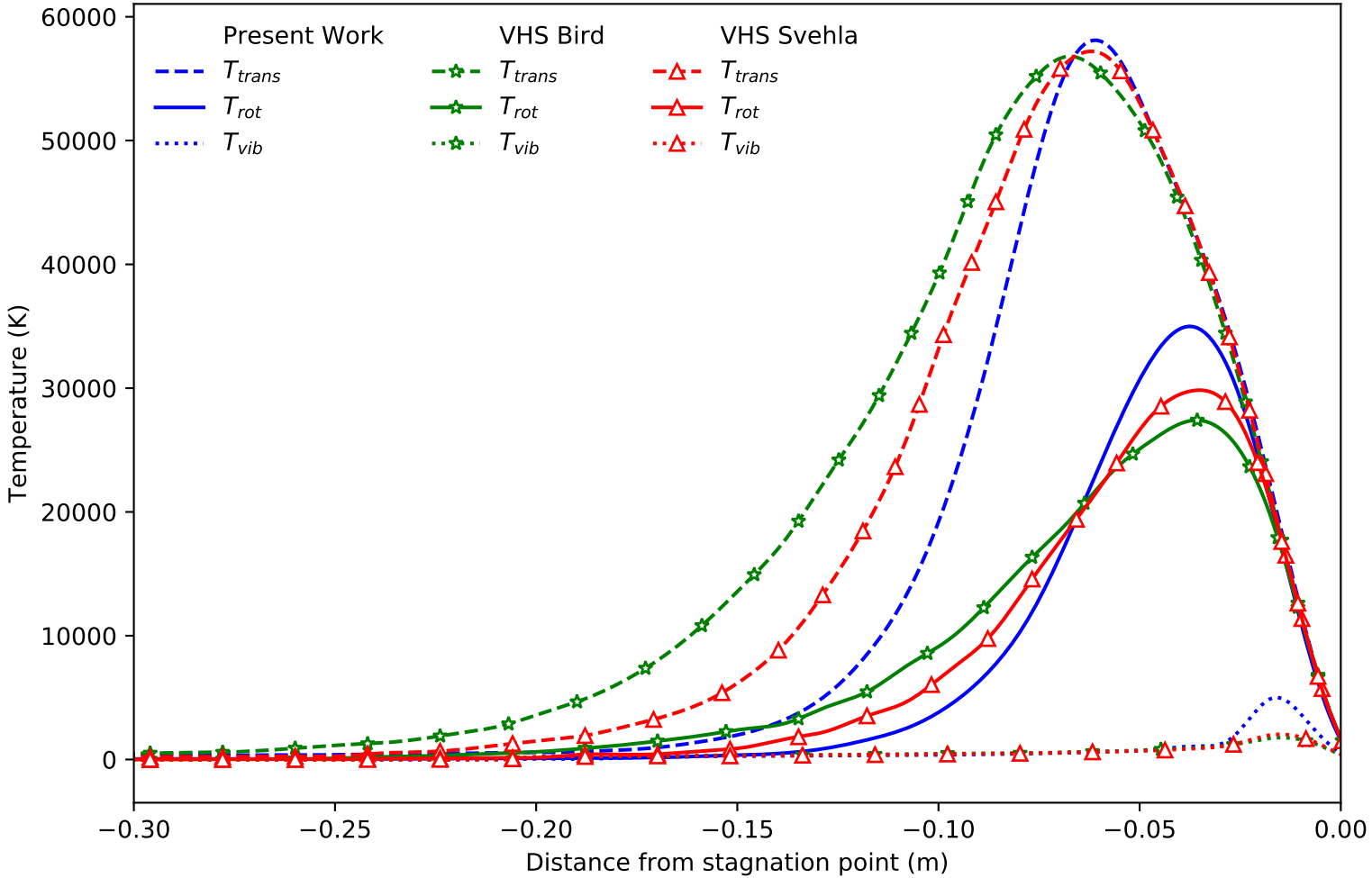
Present Work
T_{trans}
T_{rot}
T_{vib}
VHS Bird
T_{trans}
T_{rot}
T_{vib}
VHS Svehla
T_{trans}
T_{rot}
T_{vib}
Temperature (K)
60000
50000
40000
30000
20000
10000
0
−0.30
−0.25
−0.20
−0.15
−0.10
−0.05
0.00
Distance from stagnation point (m)

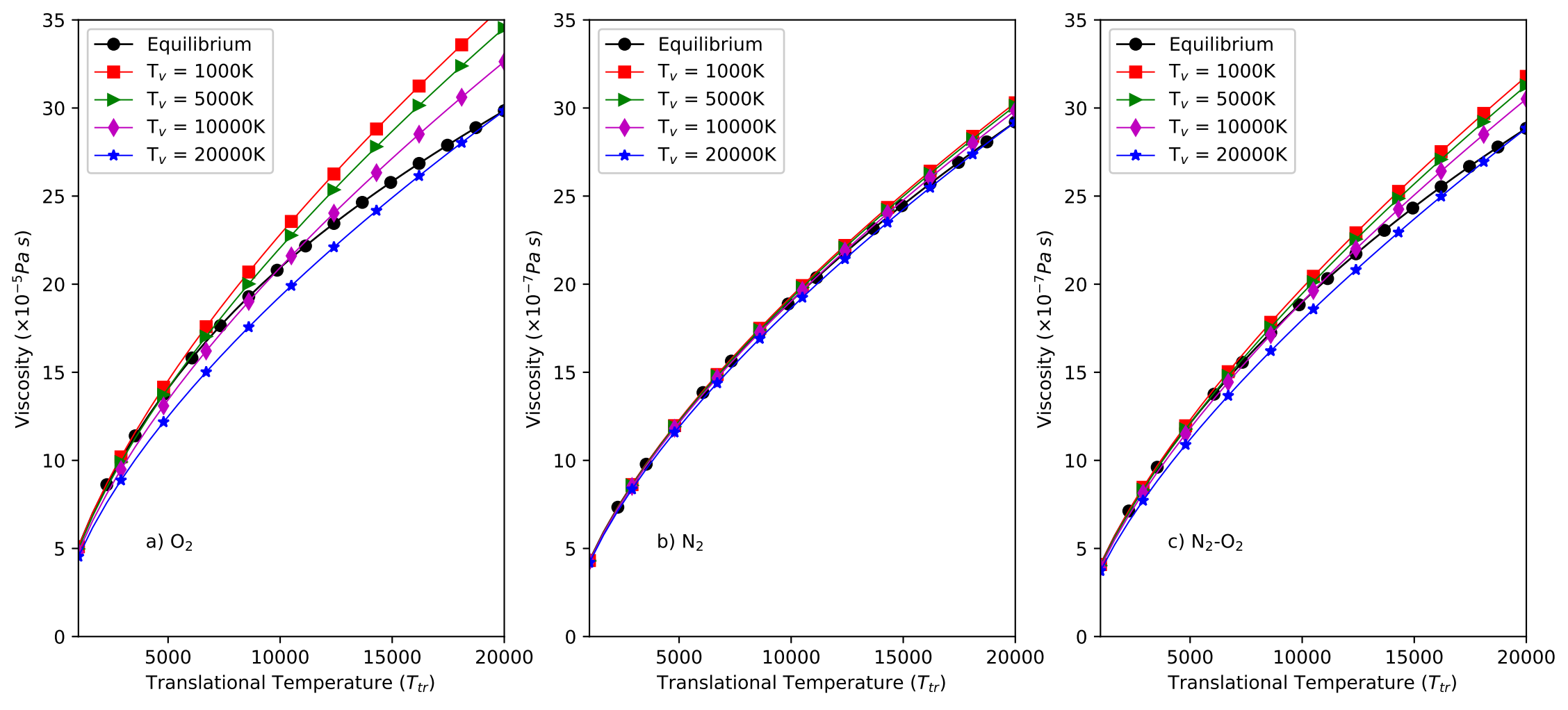
Equilibrium
T_v = 1000K
T_v = 5000K
T_v = 10000K
T_v = 20000K
Viscosity ($\times 10^{-5} Pa\ s$)
Translational Temperature (T_{tr})
a) O_2
Viscosity ($\times 10^{-7} Pa\ s$)
b) N_2
c) N_2-O_2
0
5
10
15
20
25
30
35
5000
10000
15000
20000